Measurements and model of the cat middle ear: Evidence of tympanic membrane acoustic delay

Sunil Puria[a)]
Eaton-Peabody Laboratory of Auditory Physiology, Massachusetts Eye and Ear Infirmary, 243 Charles Street, Boston, Massachusetts 02114 and Department of Otology and Laryngology, Harvard Medical School, Boston, Massachusetts 02114 and The Research Laboratory of Electronics, Massachusetts Institute of Technology, 77 Massachusetts Avenue, Cambridge, Massachusetts 02139

Jont B. Allen
AT&T Labs—Research, 180 Park Avenue, P.O. Box 971, Florham Park, New Jersey 07932-0971

(Received 16 February 1998; revised 17 August 1998; accepted 29 August 1998)

In order to better understand the mechanics of tympanic membrane (TM) transduction at frequencies above a few kHz, the middle-ear (ME) impedance measured near the tympanic membrane is studied for three anesthetized cat ears after widely opening the ME cavities (MEC). Three conditions were measured: intact ossicles, drained cochlea, and disarticulated stapes. When the cochlear load is removed from the ME by disarticulating the stapes, the impedance magnitude varies by about ± 25 dB in the 5- to 30-kHz range, with peaks and valleys at intervals of ≈ 5 kHz. These measurements suggest middle-ear standing waves. It is argued that these standing waves reside in the TM. In contrast, the magnitude of the impedance for the intact case varies by less than ± 10 dB, indicating that for this case the standing waves are damped by the cochlear load. Since the measurements were made within 2 mm of the TM, standing waves in the ear canal can be ruled out at these frequencies. Although the ME cavities were widely opened, reflections from the ME cavity walls or surrounding structures could conceivably result in standing waves. However, this possibility is ruled out by model predictions showing that such large standing waves in the ME cavity space would also be present in the intact case, in disagreement with the observation that standing waves are damped by cochlear loading. As a first-order approximation, the standing waves are modeled by representing the TM as a lossless transmission line with a frequency-independent delay of 36 μs. The delay was estimated by converting the impedance data to reflectance and analyzing the reflectance group delay. In the model the ossicles are represented as lumped-parameter elements. In contrast to previous models, the distributed and lumped parameter model of the ME is consistent with the measured impedance for all three conditions in the 200-Hz to 30-kHz region. Also in contrast with previous models, the ear-canal impedance is not mass dominated for frequencies above a few kHz. Finally, the present model is shown to be consistent, at high frequencies, with widely accepted transfer functions between (i) the stapes displacement and ear-canal pressure, (ii) the vestibule pressure and ear-canal pressure, and (iii) the umbo velocity and ear-canal volume velocity. An improved understanding of TM mechanics is important to improve hearing aid transducer design, ear-plug design, as well as otoacoustic emissions research. [S0001-4966(98)02812-4]

PACS numbers: 43.64.Bt, 43.64.Ha, 43.64.Jb [BLM]

INTRODUCTION

The tympanic membrane (TM) transduces the ear-canal sound pressure into a mechanical motion of the ossicles. The goal of the research reported in this paper is to improve our understanding of the function of the TM and other middle-ear (ME) structures. Consider the following: (1) In theory, mass inertia of the ossicles should result in an increase in ME input impedance as frequency increases (Shaw and Stinson, 1981), and (2) surface displacement patterns of the cat TM suggest that above a few kHz the TM surface has modes (i.e., standing waves) (Khanna and Tonndorf, 1972). In both of these cases the coupling of the ear-canal sound pressure to the ossicles will effectively decrease as stimulus frequency increases above a few kHz. The basic question asked by this paper is: *How does the TM couple sound into the cochlea above a few kHz?*

Figure 1 shows the ME input impedance $Z_{ec}(\omega)$ measured close to the TM with middle-ear cavities (MECs) wide open, for three different conditions: (I) intact middle and inner ear, (II) drained cochlea, and (III) disarticulated stapes. In the disarticulated stapes and drained-cochlea cases, the impedance magnitude periodically increases and decreases by as much as ± 25 dB [Fig. 1(C) and (E)], indicative of low-loss standing waves. In the intact case these standing waves are damped by the cochlea [Fig. 1(A)]. The figure shows that the standing waves are significantly damped in all three ears measured. These results suggest that the ME supports the propagation of low-loss traveling waves, and that the damping of these waves is provided by cochlear loading.

[a)]Electronic mail: purial@leland.Stanford.edu

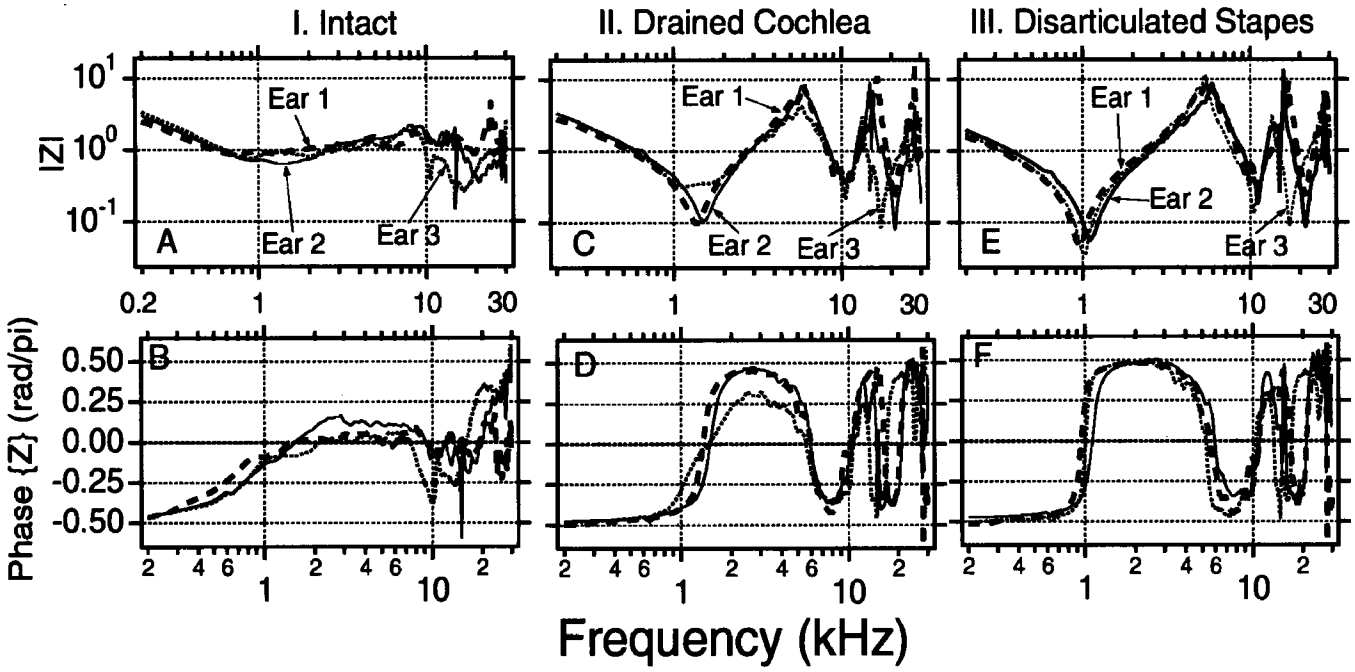

FIG. 1. The middle-ear (ME) input impedance was measured by placing a calibrated sound-delivery tube and microphone assembly within 2 mm of the TM surface with the bulla wall wide open and the bony septum removed. Measurements in three cat ears, from 0.2 to 30 kHz, are shown. Impedance measurements of Z_i, Z_{dc}, and Z_{ds} were made in the following order: (I) intact: ossicles and cochlea in their normal state (Z_i), (II) drained cochlea: scala-vestibule and scala-tympani perilymph removed (Z_{dc}), and (III) disarticulated stapes: cut stapes away from incus at the incudo-stapedial joint (Z_{ds}). The top panels (A,C,E) show impedance magnitudes, normalized by the characteristic impedance of the transducer sound-delivery tube $Z_{ot}=400$ ohms (dyne-s/cm^5). The bottom panels (B,D,F) show phase angles of the impedance in rad/π (e.g., ± 0.5 rad/$\pi=\pm 90°$). In all figures, the line types of the unlabeled panels are identical to the line types of the labeled panels (e.g., the solid line corresponds to ear 2 in panels B and A).

Thus a primary problem posed in this paper is how do we understand these measurements? The answer will lead to a better understanding of the TM with respect to high-frequency ME sound transmission.

To study the question of ME sound transmission, ME input impedance was transformed to reflectance magnitude and reflectance group delay. For the disarticulated stapes and drained cochlea cases, the mean group delay is approximately 100 μs in the 3–20-kHz frequency region. A delay of 100 μs corresponds to the round-trip delay in a 1.7-cm-long air-filled tube. Given that measurements were made within approximately 0.2 cm of the surface of the TM, standing waves in the ear canal can be ruled out for frequencies below 30 kHz. It is unlikely that there are standing waves (i.e., large delays) in the ossicles. Thus a secondary question posed in this paper is: *How can we account for the large delays measured in the middle ear?* Since the cochlea is removed by disarticulating the stapes, these 100-μs delays cannot originate from the inner ear.

Attempts to understand the data of the type shown in Fig. 1 with standard lumped parameter model representations for the TM (Zwislocki, 1962; Møller, 1965; Matthews, 1983) have been successful for frequencies below 6–8 kHz, but fail at the higher frequencies (Puria, 1991b). Existing ME models (Flanagan, 1962; Zwislocki, 1962, 1963; Peake and Guinan, 1967; Nuttall, 1974; Shaw and Stinson, 1981; Kringlebotn, 1988; Shera and Zweig, 1991; Goode *et al.*, 1994) are also limited at frequencies above approximately 8 kHz (Rabbitt and Holmes, 1986, 1988). Finite-element models have been previously proposed to circumvent this problem (Funnell *et al.*, 1987). In the present work we explore a more parsimonious solution by using a distributed parameter (i.e., transmission line) model.

Two likely hypotheses for the measurements shown in Fig. 1 are presently explored: (1) standing waves in the tympanic membrane, or (2) standing waves in the open MEC space. Mathematical models constrained by measurements are used to explore both hypotheses. We conclude that the MEC model is inconsistent with measurements, and thus can be ruled out.

It follows that the physical mechanism for the observed 100-μs delay is TM transverse wave propagation. We show (i) to a first-order approximation the TM can be modeled as a transmission line with a frequency-independent delay, and (ii) the TM model, along with a lumped–parameter representation of the ossicles, is consistent with both the ME input impedance data shown in Fig. 1, as well as with numerous physiological measurements of the cat ME reported in the literature. Model calculations, valid to at least 25 kHz, are for a single set of parameters. A preliminary version of this paper was previously presented (Puria and Allen, 1996).

I. METHODS

A. Preparation

Methods of animal preparations have been previously described (Allen, 1983). Briefly, the bulla cavity was widely opened and the bony septum that separates the bulla cavity from the tympanic cavity removed (Fig. 2). The ear canal was surgically removed and a calibrated receiver and probe-

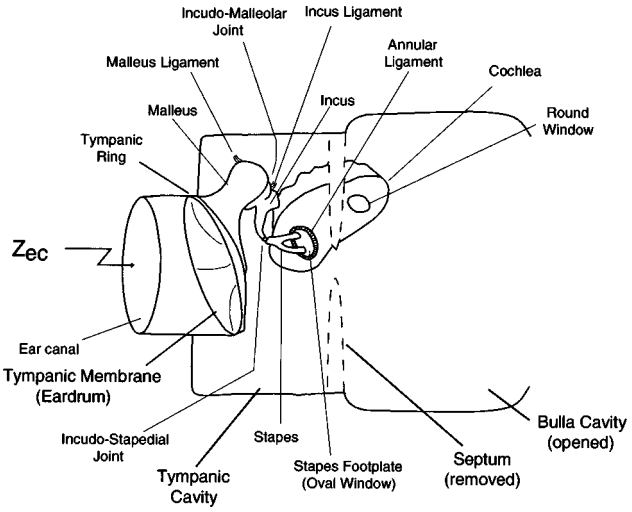

FIG. 2. Simplified cat ME anatomy. The bulla cavity was widely opened and the septum removed (dashed line). The ear-canal impedance was measured by placing a calibrated microphone and sound delivery system in the ear canal close to the TM. The impedance was measured for the intact ossicles, after draining the cochlea and after disrupting the ossicular chain by cutting the incudo-stapedial joint. The malleus and incus are attached to the walls of MEC space by the malleus and incus ligaments.

tube microphone assembly was put in place near the bony end of the ear canal (the microphone probe tube was typically less than 2 mm from the surface of TM).

Following the ear preparation, the ME input impedance and cochlear microphonic (CM) were measured. The acoustic impedance calibration of the sound delivery system has been previously described (see Sec. I B). The sound delivery system was always calibrated at the start of each impedance measurement session. If either the CM or the ME impedance showed any indication of a bulla resonance, the bulla was opened more widely and the impedance remeasured until there were no indications of a ME cavity resonance. Once the experimental series of cochlear and ME modifications was started, no further modifications to the MECs were made.

B. Measurements

The definition of impedance is based on the assumption that the ear-canal pressure, in the measurement plane, is independent of spatial location; in other words, higher-order spatial modes are assumed to be negligible. Complex wave motions on the TM result in higher-order evanescent modes near the eardrum which complicate measurements of impedance. Theoretical arguments suggest that for distances greater than 0.15 cm, and for frequencies below 25–30 kHz, the effect of these evanescent modes on the ear-canal pressure is insignificant (Lynch, 1981, pp. 146–148; Stinson, 1994).

TABLE I. Constants presently assumed and shown below are valid for 27 ± 10 °C: ρ_a is the mass density of air; c_a is the speed of sound in air, A_t is the area of the sound delivery tube, and $Z_{ot}=\rho_a c_a/A_t$ is the characteristic impedance of the sound delivery tube.

ρ_a	1.177×10^{-3}	g/cm^3
c_a	3.472×10^{4}	cm/s
A_t	0.102	cm^2
Z_{ot}	400	dyn-s/cm^5

Ear-canal pressure measurements were made for frequencies up to $33\frac{1}{3}$ kHz with a frequency resolution of 65.1 Hz and 512 frequency points (the response at 0 Hz was not measured) using the SYSid™ (Puria and Allen, 1992; Puria *et al.*, 1993) measurement and analysis system (SYSid Labs, Berkeley, CA). A 1024-point buffer with a chirp stimulus sampled at a rate of 15 μs was used. As described elsewhere (Allen, 1983), cochlear microphonic measurements were also made on these ears using tones.

The four-load impedance measurement technique was used. This method was developed by Allen (1986), and has been previously described (Allen, 1986; Puria, 1991b; Keefe *et al.*, 1992; Voss and Allen, 1994). Briefly, the Thévenin source impedance $Z_0(\omega)$ and source pressure $P_0(\omega)$ of the sound delivery system are estimated by measuring the probe microphone pressure responses to four known acoustic loads.[1] The ME acoustic impedance may then be calculated directly from measured ear-canal pressure and the Thévenin source parameters $Z_0(\omega)$ and $P_0(\omega)$. Throughout this paper all Thévenin and ME input impedance measurements have been normalized by the characteristic impedance $Z_{ot}=\rho_a c_a/A_t=400$ (cgs-ohms) of the sound delivery tube (see Table I).

C. Impedance minimum-phase test

Impedance measurement techniques require that Thévenin (or Norton) equivalent parameters for the source do not change from the time of calibration to the time of measurements. Measurement errors otherwise occur. The source characteristics will change, for example, if the temperature changes. A procedure to check for possible inconsistencies in impedance measurements, by checking the ratio of the Thévenin source pressure to the ear-canal pressure $H(\omega)\equiv P_0(\omega)/P_{ec}(\omega)$ for minimum-phase behavior, was outline by Voss and Allen [1994, Eqs. (15)–(17)]. $H(\omega)$ for the data reported here was checked for their minimum-phase property. It was found that $H(\omega)$ had an all-pass delay of 2–4 μs, and thus was not minimum phase. This all-pass delay corresponds to less than $\frac{1}{3}$ of a Nyquist sample at the 15-μs Nyquist rate, and this delay error can be accounted for by the difference in temperature of the sound delivery system at the time of calibration (room temperature) and temperature of the sound delivery system at measurement time (animal body temperature). All the data shown here have been corrected by subtracting a delay of 2–4 μs such that the pressure ratio $H(\omega)$ is minimum phase for frequencies below about 25 kHz. This guarantees that the ear-canal impedance is minimum phase.

D. Middle-ear modifications

The ME input impedance was measured in approximately 27 animals, but the complete set of measurements,

(I) the intact ear—$Z_i(\omega)$,

(II) perilymph removed—''drained cochlea'' $Z_{dc}(\omega)$, and

(III) ''disarticulated stapes''—$Z_{ds}(\omega)$ by cutting at the incudo-stapedial joint,

was obtained on 3 ears (two animals), reported here.[2]

All of these measurements are with the MEC wide open, as described in Sec. I A. The cochlea was drained by removing the round–window membrane, and wicking out the scala-tympani perilymph. The basilar membrane was next removed, allowing the scala-vestibule perilymph to drain via the wick. The disarticulated stapes case was measured after cutting at the incudo-stapedial joint. Several intermediate impedance measurements were made, but are not reported here (Allen, 1986). All surgical modifications and measurements were performed by the second author, following the technique and guidance of J. Tonndorf (Tonndorf and Pastaci, 1986).

II. FROM IMPEDANCE TO REFLECTANCE

A. Impedance

Normalized impedance measurements from ears 1–3, shown in Fig. 1, have a similar pattern for any given condition. For frequencies below about 800 Hz the impedance is stiffness dominated for all three cases, and the magnitude is larger for the drained cochlea [panel (C)] than for the disarticulated stapes case [panel (E)]. This difference in stiffness represents the additional stiffness of the annular ligament. Note also that the phase for the disarticulated case is more bimodal (i.e., reactive) than that of the drained case due to the removal of annular ligament damping.

The drained cochlea [panels (C) and (D)] and disarticulated stapes [panels (E) and (F)] cases clearly show standing waves (i.e., high-Q low-loss modes). For example, panel (C) near 6 kHz shows a local maximum in the impedance magnitude while the phase data in panel (D) shows a corresponding phase shift from $+0.5$ to -0.5 rad/π. Given the ± 25 dB variations in impedance magnitude (the peaks and valleys) we may conclude that the ME damping is quite small. Since the stapes, annular ligament, and cochlea are not present for the disarticulated case, it is clear that these structures are not responsible for the standing waves. What is surprising about these figures, besides the low damping of the isolated ME, is the large ME delays that must be present to produce these standing waves with such low resonant frequencies.

Panels (A) and (B) show that the cochlear load dampens the standing waves because of the energy absorbed by the cochlea (Møller, 1965; Lynch, 1981; Tonndorf and Pastaci, 1986). This is consistent with how we might imagine the ME and cochlea might function to have a reasonable efficiency.

Since the magnitudes of the ME impedances for the three ears have multiple maxima and minima that are not exactly at the same frequency, there is no simple way to shift the impedances so that all the maxima and minima are aligned. Averaging these data would smear these peaks and valleys, which would result in a loss of data features. Rather than average data, we have used ear 1 as a prototypical example for modeling purposes.[3] The best middle ears, defined as having the smoothest impedance frequency responses, the widest frequency bandwidth, and the largest cochlear microphonic to drum pressure ratios over frequency, correspond to clean transparent ear drums.

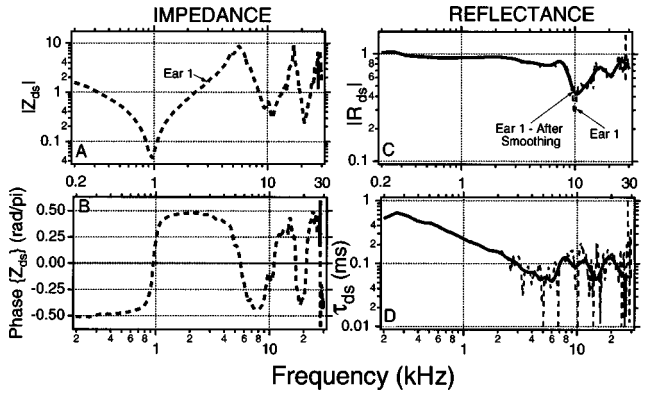

FIG. 3. Disarticulated stapes for ear 1. (A) Normalized impedance magnitude, and (B) phase in rad/π. (C) Reflectance magnitude before and after smoothing. (D) Reflectance group delay before and after smoothing the reflectance phase and then using Eq. (4) to calculate the group delay. For both magnitude and phase, recursive-exponential smoothing filters were used (see text).

B. Reflectance

The ME impedance measured near the TM, normalized by the characteristic impedance of the transducer sound-delivery tube (Z_{ot}), is defined as $Z_{me}(\omega)$. This normalized impedance may be expressed in terms of the pressure reflectance (Puria and Allen, 1989; Puria, 1991a, b; Keefe *et al.*, 1992, 1993; Voss and Allen, 1994)

$$R(\omega)=\frac{Z_{me}(\omega)-1}{Z_{me}(\omega)+1}, \tag{1}$$

where

$$R(\omega)\equiv\frac{P_-}{P_+} \tag{2}$$

$$=|R(\omega)|e^{j\angle R(\omega)}. \tag{3}$$

In Eq. (2) the pressure reflectance is defined as the transfer function between the retrograde $P_-(\omega)$ and incident $P_+(\omega)$ pressure waves. In Eq. (3) the reflectance is expressed in polar coordinates in terms of a magnitude $|R|$ and phase angle $\angle R$.

The group delay of the reflectance

$$\tau(\omega)\equiv-\frac{\partial\angle R(\omega)}{\partial\omega} \tag{4}$$

is a measure of the delay between the retrograde pressure wave $P_-(\omega)$ and the incident pressure wave $P_+(\omega)$ (Puria and Allen, 1989; Puria, 1991a, b; Voss and Allen, 1994). In other words, group delay is a measure of the latency of the reflected sound relative to the incident sound; this interpretation is restricted to frequency regions where the derivative

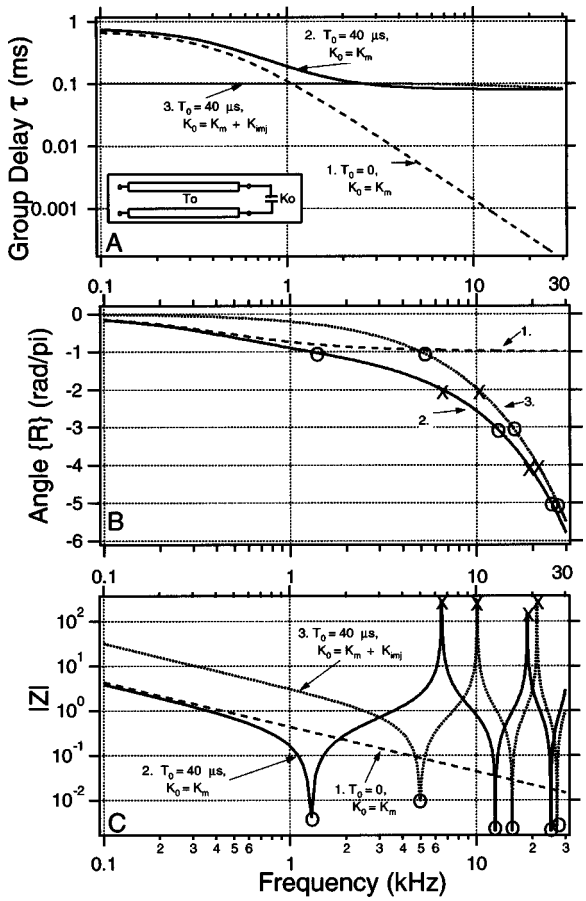

FIG. 4. Three examples of a simple middle-ear model consisting of a lossless transmission line having a frequency-independent delay T_0, terminated by a stiffness K_0, as defined in the insert. This model illustrates the point that the frequency location of the maxima and minima (poles and zeros) of the impedance depends mainly on the group delay of the reflectance. The three examples are: (1) $T_0=0$ (e.g., no transmission line), $K_0=K_m=1.1\times10^6$ (dyn/cm^5), (2) $T_0=40$ μs, $K_0=K_m$, and (3) $T_0=40$ μs, $K_0=K_m+K_{\text{inj}}=3.81\times10^7$ (dyn/cm^5). (A) The group delay of the reflectance for the three cases. (B) The phase of the reflectance is computed from the integral of the group delay [Eq. (10)]. (C) The ○'s indicate location of zeros while ×'s indicate location of poles of the impedance. The frequency of the zeros is when the reflectance phase is at odd multiples of π, while the frequency of the poles is at even multiples of π. As the amount of delay increases, the accumulated reflectance phase increases and the pole-zero frequency spacings of the impedance decrease.

of $|R(\omega)|$ with respect to frequency is small (Papoulis, 1962, p. 135). Given the above view point, reflectance is a measure that is conceptually related to transient evoked otoacoustic emissions. In the present case the reflectance is derived from measurements using chirps, rather than clicks.

In Fig. 3, panels (A) and (B) show the impedance for the disarticulated stapes case of ear 1, panel (C) shows the corresponding reflectance magnitude, while panel (D) shows the reflectance group delay (dashed lines). The reflectance magnitude $|R(\omega)|$ [Fig. 3(C)] is typically greater than 0.4 for all frequencies measured and is greater than 0.8 for frequencies below 8 kHz. The group-delay data for the disarticulated stapes case [Fig. 3(D)] decreases from about 0.5 to 0.1 ms as frequency increases from 0.2 to 3 kHz. At frequencies above 3 kHz the group delay on the average stays near 0.1 ms. Although there are trends for frequencies above 3 kHz, the group delay shows greatly increased variability (dashed lines).

1. Smoothing of reflectance data

To better analyze the trends in the reflectance group delay, the phase of the reflectance was first smoothed using recursive-exponential filters (Shera and Zweig, 1993, Appendix). These filters avoid prolonged ringing in the frequency domain while minimizing splatter in the time domain.[4] Equation (4) was then used to compute the group delay. The reflectance magnitude was also smoothed with the same recursive-exponential filters. It is evident from the group delay after smoothing [Fig. 3(D), solid line] that there are systematic variations in the delay. These variations are related to the variability in reflectance magnitude above 3 kHz which is likely due to radiation from the back side of the TM (see the Appendix). Below approximately 2 kHz, the delay estimates have a small variance. Group delay for the drained inner-ear and intact cases will be discussed after the full ME model is presented.

III. A SIMPLE MIDDLE-EAR MODEL: A PRELUDE

In this section we present a greatly simplified ME model, shown in the insert of Fig. 4(A). With this lossless and massless model, consisting of a TM as a transmission line with delay T_0 terminated by stiffness K_0, we can account for much of the observed ear-canal reflectance group delay $\tau(\omega)$ for the modified ME conditions for a wide range of frequencies. We then proceed to show how the ME impedance is related to the group delay using Eqs. (1) and (4), along with the lossless assumption $|R(\omega)|=1$.

A. Modeling the group delay $\tau(\omega)$

It is widely accepted that the ear-canal impedance is stiffness dominated below a few kHz (Onchi, 1961; Zwislocki, 1962; Møller, 1965). By substituting the stiffness-dominated TM impedance $K_{\text{tm}}/j\omega$ into Eq. (1), and using the definition of $\tau(\omega)$ given by Eq. (4), Voss and Allen (1994) found a formula for the reflectance group delay. In their formulation, a transmission line representing the ear canal is terminated by a compliance representing the TM stiffness K_{tm}. Generalizing the Voss and Allen (1994) model to include the proposed TM delay, we model the ear canal and TM as a uniform tube, having a characteristic impedance Z_{ot} and an effective acoustic delay T_0, terminated by an effective stiffness K_0 [as shown in Fig. 4(A) insert].

The reflectance for this simplified model is

$$R(\omega)=\frac{1-j\omega\tau_c}{1+j\omega\tau_c}\,e^{-j\omega 2T_0}, \tag{5}$$

where

$$\tau_c=Z_{ot}/K_0. \tag{6}$$

The group delay $\tau(\omega)$ for the model represented by Eq. (5) is (Voss and Allen, 1994)

$$\tau(\omega)=2T_0+\frac{2\tau_c}{1+(\omega\tau_c)^2}. \tag{7}$$

Equation (7) predicts a high-frequency round trip delay of $\tau(\omega\rightarrow\infty)=2T_0$, and a low-frequency round trip delay of $\tau(\omega\rightarrow 0)=2T_0+2\tau_c$. Thus the total delay consists of the sum of a low-frequency delay below f_c, and a fixed wideband delay, where

$$f_c \equiv 1/2\pi\tau_c . \tag{8}$$

From this definition and Eq. (7) we find

$$\tau(2\pi f_c)\equiv 2T_0+\tau_c . \tag{9}$$

From Fig. 3(D) we see a delay which is qualitatively similar to the prediction of Eq. (7). At high frequencies the terminating compliance has an impedance that is much smaller than the characteristic impedance of the transmission line, and the termination reflects all the energy above that frequency with the round trip line delay of $2T_0$. At low frequencies, defined as $f<f_c$, the transmission line has an effective acoustic length that is longer than $2T_0$ due to the terminating compliance (Voss and Allen, 1994).

Equations (7)–(9) are important because they separate the delay of the transmission line T_0 from the delay due to the terminating stiffness K_0. If the TM operates as a delay line, then its delay appears as an extension of the canal delay line, rather than as part of the stiffness of the ossicles. Thus this model allows us to address one of the basic issues of the physical properties of the tympanic membrane: *Is the TM best modeled as a combination of a few stiffness, mass, and damping elements, or as a transmission line?*

1. An estimate of the TM delay

An approximation to the TM delay may be obtained using previously established ossicle stiffness values, the group delay shown in Fig. 3(D), and the equations for the simple ME model [Fig. 4(A) insert] outlined above.

Below about 1 kHz the ossicle impedance is dominated by the ligament stiffness, and the element impedances are approximately known. Based on an extensive series of cat middle-ear impedance measurements, Lynch (1981, pp. 226–231) estimated the malleus-ligament stiffness $K_{\rm m}$ (1.1×10^6 dyn/cm^5) and the IM joint stiffness $K_{\rm imj}$ (37×10^6 dyn/cm^5).

For the disarticulated stapes case, the stiffness of the malleus is dominated by the anchoring ligaments $K_0=K_{\rm m}$. Using $K_{\rm m}=1.1\times 10^6$ (dyn/cm^5), we find $\tau_c=365$ μs from Eq. (6), and $f_c=437$ Hz from Eq. (8). Using this cutoff frequency, the delay $\tau(f_c)$ for the disarticulated stapes case [Fig. 3(D)] is 0.45 ms. From Eq. (9) we estimate the TM and ear-canal delay T_0 to be 42.5 μs.

For the measurements shown in Fig. 1, the ear-canal space is estimated to be approximately 1.5 mm, corresponding to an ear-canal propagation delay of 4.3 μs. Subtracting this delay from the combined ear-canal and TM-delay estimate requires that the TM delay is $\approx$38 μs. The distance corresponding to this delay for sound propagation in air is 1.3 cm, which is significantly larger than the physical dimensions of the tympanic membrane. Thus, the above theoretical considerations, combined with previous middle-ear measurements, suggest that there is significant delay in the tympanic membrane. It follows that the velocity of wave propagation must be slower than the speed of sound in air, by an amount that is $\approx$3.6 (radius of 0.36 cm).

B. Examples of the simple model

In this section we illustrate how the frequency spacing of the poles (maxima) and zeros (minima) of the ME impedance of the delay and stiffness model depends on the reflectance delay and terminating stiffness. Three examples are given: (1) a pure stiffness, (2) a short piece of transmission line terminated with a stiffness, and (3) same as case 2 but with increased stiffness. This last case corresponds to ''blocked incus.'' Finally the impedance is computed from the group delay using the reflectance formula Eq. (1) with no losses (i.e., $|R|=1$). In these three examples the group delay $\tau(\omega)$ is the only model parameter (as dictated by T_0 and K_0). The delay and phase are calculated from model equation (7), while the loss is set to zero.

1. Group delay

The group delay of the simple model [Fig. 4(A) insert] consisting of a lossless transmission line with delay T_0 and a terminating impedance determined by stiffness K_0 is shown in Fig. 4(A), for three different conditions. In the three examples the group delay of the reflectance is given by Eq. (7). We use Lynch's parameters for $K_{\rm m}$ and $K_{\rm imj}$ and TM delay estimated in the previous section.

For example 1 the stiffness is $K_0=K_{\rm m}=1.1\times 10^6$ (dyn/cm^5) and $T_0=0$ (e.g., no transmission line). Using Eq. (6) we find that τ_c is 365 μs. Thus, as shown in Fig. 4(A), the reflectance delay asymptotically approaches 730 μs as frequency decreases. According to Eq. (8) the cutoff frequency f_c is approximately 435 Hz. Above f_c, the delay decreases by a factor of 4 for each octave increase in frequency.

For example 2, we add a transmission line with delay $T_0=40$ μs to the stiffness $K_0=K_{\rm m}$. According to Eq. (7), when a transmission line is terminated with stiffness $K_{\rm m}$, one simply adds the delay of the transmission line to the delay due to the stiffness alone to obtain the total delay. This is graphically illustrated in Fig. 4(A). The group delay for example 2 is always greater than for example 1.

If we assume that the malleus mass and all middle-ear losses are negligible, then example 2 approximates the disarticulated stapes case. This is apparent from the comparisons of the group delays shown in Figs. 3(D) and 4(A).

In example 3, the incudo-malleolar joint stiffness $K_{\rm imj}=3.7\times 10^7$ (dyn/cm^5) is added to the malleus stiffness (e.g., $K_0=K_{\rm imj}+K_{\rm m}$) terminating the $T_0=40$ μs transmission line. Example 3 is similar to example 2 except that the incudo-malleolar joint stiffness is added to the malleus stiffness. Thus stiffness K_0 is more than an order of magnitude greater for example 3 than for example 2. This example corresponds to the incus blocked at the IS joint. For this case τ_c is approximately 10.5 μs [Eq. (6)]. At low frequencies we expect the delay $\tau(0)=2T_0+2\tau_c$ to be 101 μs. At high frequencies the reflectance delay τ should decrease to $2T_0=80$ μs with a cutoff frequency f_c of 15 kHz.

2. From reflectance back to impedance

The reflectance group delay determines the reflectance phase, which in turn determines the location of the poles and zeros of the impedance. The magnitude of the reflectance, on the other hand, determines the bandwidths of the poles and zeros. This follows from two formulas: the integral of Eq. (4),

$$\angle R(\omega) = -\int_0^{\omega} \tau(\omega)\, d\omega \tag{10}$$

for $\omega > 0$, and

$$Z_{\mathrm{me}}(\omega) = \frac{1+|R(\omega)|e^{j\angle R(\omega)}}{1-|R(\omega)|e^{j\angle R(\omega)}}, \tag{11}$$

which follows from Eqs. (1) and (3). The group delay may be transformed into a reflectance phase angle by using Eq. (10). As frequency increases, the phase angle increases (assuming a positive group delay), and $R(\omega)$ rotates about the origin in the complex plane. When R is close to ± 1, the impedance Z_{me} shows poles, defined as the set of complex frequencies $s_n = \sigma_n + j\omega_n$ where $R(s_n) = 1$, and zeros, defined by $R(s_n) = -1$.

Since the magnitude of the reflectance is close to one for conditions when the cochlear load is removed from the middle ear, to a first-order approximation, we can model the impedance over a wide range of frequencies given only the group delay data.

In example 1 there is no added delay; thus the reflectance angle asymptotically approaches π as frequency increases (e.g., $\angle R(\omega)|_{\omega\to\infty} \to \pi$) and asymptotically approaches 0 as frequency decreases (e.g., $\angle R(\omega)|_{\omega\to 0} \to 0$). Thus there is a zero in the impedance as $\omega \to \infty$ and a pole in the impedance as $\omega \to 0$. Note that by simply adding delay (example 2), multiple maxima and minima are introduced in the impedance magnitude above 1 kHz. Example 1 thus demonstrates that, when there is insufficient delay, the reflectance phase angle [Eq. (10)] rotates about the origin so slowly that the poles and zeros of Eq. (11) occur with a much wider frequency spacing. When there is delay (as in the case in examples 2 and 3), the poles and zeros in the ME impedance occur due to standing waves in the transmission line. In this simple model there are no losses (e.g., $|R| = 1$) and thus the poles and zeros have infinite Q's. More realistically $|R| < 1$, and, correspondingly, the bandwidth increases and the Q's having finite values.

In summary, addition of group delay to the reflectance is the key to a model that works over a wide frequency range, as shown by our three simple examples.

IV. THE MIDDLE-EAR MODEL

Up to this point we have explored the possibility that there is delay in the tympanic membrane. In this section we formulate a more complex model that allows us to investigate the possibility that the measured ear-canal reflectance delay is in the residual postsurgical, widely opened ME cavity.

Middle-ear models are commonly defined in terms of lumped-parameter (parametric) models. We shall follow this approach with three significant exceptions. We represent the measured delay [Fig. 3(D)] first as delay in the TM, and second as delay in the middle-ear cavity. Third, we define the cochlear impedance in nonparametric terms as $Z_c(\omega)$. The remaining elements are described as lumped-parameter elements.

A. Description of the models

The motions of the middle ear can be described by the general model of Fig. 5(A) consisting of three basic components: (1) the residual ear-canal space between the tip of the probe-tube microphone and the tympanic membrane, (2) the radiation impedance due to the residual ME cavity $Z_{\mathrm{mec}}(\omega)$, and (3) the ossicular chain impedance $Z_{\mathrm{oc}}(\omega)$ due to the TM, the ossicles and cochlea. In Fig. 5(A) the MEC and the ossicular chain impedances appear in series. This assumption has been previously shown to be valid for a wide range of frequencies [Lynch, 1981 (Chap. II); Puria, 1991b (pp. 133–135)].

Figure 5(B) shows the detailed electrical circuit representation for the tympanic membrane, ossicles, and the middle-ear cavity. In Fig. 5(B) the TM and the MEC, enclosed by the dashed box, represent delay in the TM and the radiation load impedance of the open MEC. Thus the circuit of Fig. 5(B) allows us to test the TM-delay hypothesis. To test the MEC-delay hypothesis, the components in the dashed box of Fig. 5(B) are replaced by the components in the dashed box shown of Fig. 5(C).

In Fig. 5, currents and voltages of the acousto-mechanical system correspond respectively to either volume velocities and pressures, or ''particle'' velocities and forces.

1. The ear canal

The ear canal is represented by a lossy cylindrical tube (i.e., an acoustic transmission line) of length L_{ec} and diameter D_{ec}. The ear canal and the open ME cavity are separated by the TM and thus they must have the same volume velocity U_{tm}, resulting in a series configuration for the two impedances (i.e., $Z_{\mathrm{oc}} + Z_{\mathrm{mec}}$) that terminate the ear-canal space.

2. Middle-ear cavity radiation impedance

For the TM-delay hypothesis the ME cavity impedance Z_{mec} is represented by a radiation load impedance

$$Z_{\mathrm{mec}} = \frac{j\omega M_{\mathrm{rl}} \times R_{\mathrm{rl}}}{(R_{\mathrm{rl}} + j\omega M_{\mathrm{rl}})}. \tag{12}$$

In Eq. (12) M_{rl} is the mass of the radiation load and R_{rl} is the effective damping due to loss of energy through the widely opened ME cavity.[5] Equation (12) represents the functional form for either a plane piston in an infinite baffle or of a plane piston at the end of a long tube (Beranek, 1954, pp. 124–125). Our case seems to lie somewhere between these two extremes.

3. Tympanic membrane model

The ligaments of the malleus and the attachment of the anterior process of the malleus to the tympanic bone helps to

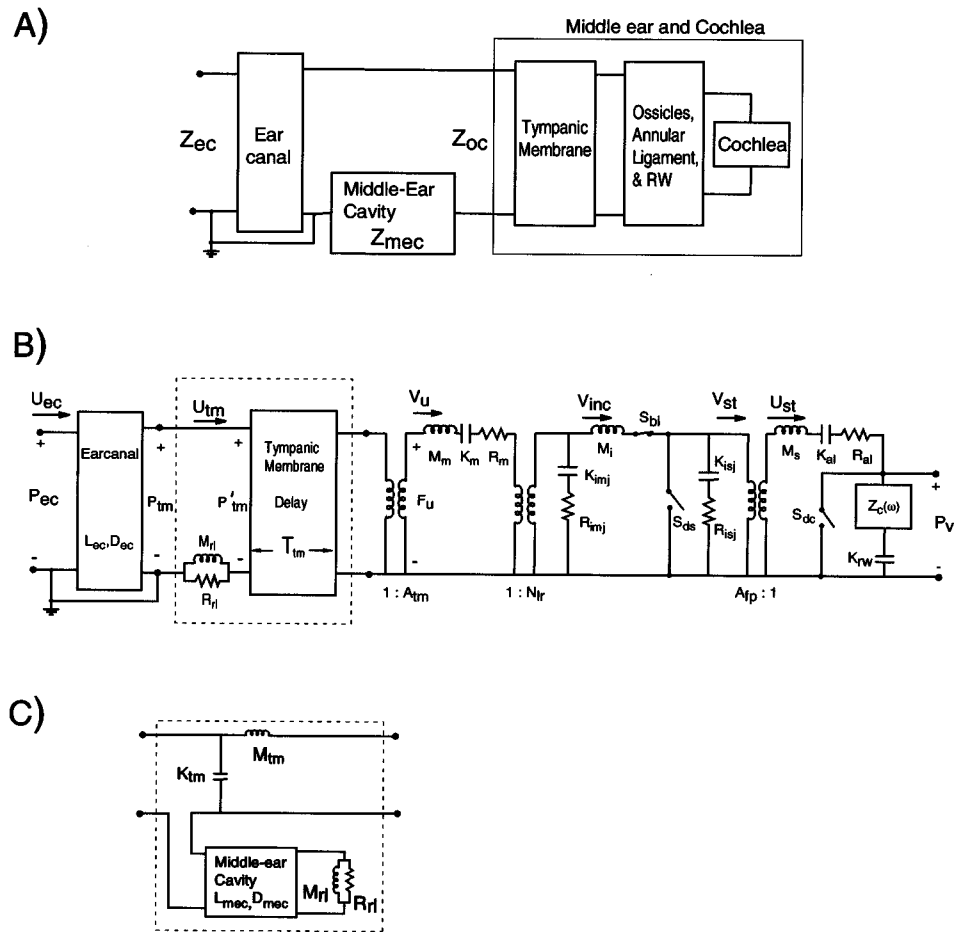

FIG. 5. Three middle-ear model circuit representations. (A) The ear-canal impedance Z_{ec} is the sum of the impedance of the middle-ear cavity Z_{mec} and the impedance of the ossicular chain Z_{oc}, which is a function of the properties of the tympanic membrane (TM), ossicles, and the cochlea. Panels B and C show two different models proposed for the TM and MEC. (B) The tympanic membrane is represented by a nondispersive lossless transmission line. This transmission line has a frequency-independent delay T_{tm} from the tympanic ring to the umbo and characteristic impedance Z_{ot}. The space between the measurement plane and the TM is represented by a cylindrical tube with diameter D_{ec} and length L_{ec}. The radiation impedance of the open middle-ear cavity is represented by the parallel combination of R_{rl} and M_{rl}. The rotational mass of the malleus is represented by M_m while malleus and incus ligaments (Fig. 2) are represented by stiffness K_m. See the text for a description of the other circuit elements. The three different measurement conditions of Fig. 1 are modeled by appropriate setting of switches S_{dc} and S_{ds}: when both switches are open, the circuit represents the intact measurement condition. With switch S_{dc} closed and S_{ds} open, the circuit represents the drained cochlea measurement condition. With switch S_{ds} closed the circuit represents the disarticulated stapes measurement condition. The third switch S_{bi} corresponds to the blocked incus case, which is discussed in the text. (C) An alternative representation for the TM and MEC is shown. The MEC-delay model is obtained by replacing the contents of the dashed box of panel B with the contents of the dashed box shown in panel C. In this model the delay is in the MEC rather than in the TM. The MEC is represented as a cylindrical tube with length L_{mec} and D_{mec} terminated by a radiation impedance. The TM is represented by a piston having stiffness K_{tm} and mass M_{tm}. The parameters for both models are listed in the Appendix.

maintain the conic shape of the TM. Békésy (1960, p. 195) has argued that the human eardrum resembles a stiffened cone rather than a stretched membrane.

The ossicular chain and TM components of the impedance is defined as Z_{oc}. In the model of Fig. 5(B) the TM is represented as a lossless transmission line having a matched characteristic impedance Z_{ot}, and a frequency-independent delay T_{tm} between the input at the tympanic ring and the output at the umbo (i.e., the tip of the manubrium). In this representation, a small segment of the TM transmission line corresponds to an annulus of the TM. The TM model shown in Fig. 5(B) can be succinctly represented in terms of a two-port matrix as follows:

$$\begin{bmatrix} P'_{tm} \\ U_{tm} \end{bmatrix} = \begin{bmatrix} A_{tm} & B_{tm} \\ C_{tm} & D_{tm} \end{bmatrix} \begin{bmatrix} F_u \\ V_u \end{bmatrix}. \tag{13}$$

The pressure in front of the TM under the condition that the MEC is short circuited ($R_{rl}=0$ or $M_{rl}=0$) is defined as P'_{tm}. The tympanic membrane matrix elements (A_{tm}, B_{tm}, C_{tm}, and D_{tm}) in Eq. (13) are due to the product of two matrices:

$$\begin{bmatrix} A_{tm}(\omega) & B_{tm}(\omega) \\ C_{tm}(\omega) & D_{tm}(\omega) \end{bmatrix} = \begin{bmatrix} \cos(\omega T_{tm}) & jZ_{ot}\sin(\omega T_{tm}) \\ jZ_{ot}^{-1}\sin(\omega T_{tm}) & \cos(\omega T_{tm}) \end{bmatrix} \times \begin{bmatrix} A_{tm}^{-1} & 0 \\ 0 & A_{tm} \end{bmatrix}. \tag{14}$$

The diagonal matrix on the right-hand side represents the TM as a transformer, with turns ratio A_{tm}. In Eq. (14) ωT_{tm} is often written as kl in transmission line terminology, where k is the wave number (ω/c) and l is the length of the line.

TABLE II. Physical dimensions assumed for the cat middle ear.

Description	Symbol	Value	Units
Length of ear canal	L_{ec}	0.15	cm
Diameter of ear canal	D_{ec}	0.36	cm
Area of TM	A_{tm}	0.41	cm^2
Area of stapes footplate	A_{fp}	0.0126	cm^2
Ossicular lever ratio	N_{lr}	2	(dimensionless)

4. Ossicular chain impedance

In Fig. 5(B), the impedance of the malleus is represented by $Z_m(\omega)=R_m+K_m/j\omega+j\omega M_m$. Stiffness K_m and damping R_m are due to the ligaments of the malleus and incus.

The transformer with turns ratio N_{lr} represents the lever ratio between the malleus and incus. The shunt impedance $Z_{imj}(\omega)=R_{imj}+K_{imj}/j\omega$ represents the slippage at the IM joint. The incus is represented by the mass M_i. The shunt impedance $Z_{isj}(\omega)=R_{isj}+K_{isj}/j\omega$ represents the slippage at the incudo-stapedial joint. The transformer with turns ratio A_{fp} converts the stapes velocity into the footplate volume velocity. The stapes is represented by mass M_s. The annular ligament which holds the stapes in the oval window is represented by a parametric viscoelastic spring, $Z_{al}(\omega)=R_{al}+K_{al}/j\omega$.

5. Cochlear load

The ''load'' on the stapes is the cochlea, consisting of the cochlear input impedance $Z_c(\omega)$ in series with the round window impedance $Z_{rw}(\omega)$. Our 1991 model results for the cochlear input impedance with tapered scalae area cochlea and viscous perilymph (Puria and Allen, 1991, Fig. 18) were used as a cochlear load, since the actual load for the animals used in this study is unknown.

6. Middle ear cavity delay model

In Fig. 5(C) the delay in the MEC is represented by a tube terminated by a radiation load impedance [Eq. (12)]. The TM is represented by a piston with stiffness K_{tm} and mass M_{tm}. The value of K_{tm} is chosen such that it has the same impedance at low frequencies as the TM-delay model ($K_{tm}=Z_{ot}/T_{tm}$). For the MEC-delay model, the widely open ME cavity is represented by a tube of length L_{mec} and diameter D_{mec} terminated in a radiation load impedance of the same form as Eq. (12) but with different parameter values.

B. Parameter selection and reduction

For the disarticulated stapes case, the TM-delay model of Fig. 5(B) requires specification of 13 parameters, while the MEC-delay model of Fig. 5(C) requires specification of 14 parameters. Since we do not know *a priori* any of the specific parameters for the ME impedance shown in Fig. 1, our approach is to draw average parameter values from the literature as a starting point and then use an optimization procedure that varies many of the parameter values, minimizing the error [Eq. (A3)] between the model and the ear-canal impedance measurements of Fig. 1.

The four parameters shown in Table II were not adjusted by the error minimization procedure. The dimensions for L_{ec} and D_{ec} were based on the approximate location of the transducer in relation to the eardrum and ear-canal dimensions. Average values for dimensions A_{tm} and N_{rl} were taken from the literature (Wever and Lawrence, 1954).

1. The matched-impedance condition

Ossicle mass can limit the high-frequency behavior of the middle ear (Shaw and Stinson, 1981). If, however, each mass element is followed by an appropriate compliance, such that a section of ''matched'' transmission line is formed by the two elements, then ossicle mass does not limit the frequency response. Such a properly matched system will attain a wide frequency response at the price of acoustic delay. This is a necessary and favorable trade. In Fig. 5(B), two of the series masses (inductors) have corresponding shunt stiffnesses (capacitors), since the malleus mass M_m may be associated with joint stiffness K_{imj}, and the incus mass M_i may be associated with joint stiffness K_{isj}. Thus the ossicles may be viewed as a lumped-parameter transmission line [e.g., Giacoletto (1977), Chap. 8]. In addition to providing a means for achieving higher-frequency response, the number of unknown parameters may be reduced by one if we assume that the IM joint stiffness K_{imj} and the malleus mass M_m are related by their *local characteristic impedance*. In summary, the basic equation for the characteristic impedance of a lumped-parameter mechanical transmission line is

$$Z_o=\sqrt{MK}, \tag{15}$$

where M and K correspond to the elements of the series mass and shunt stiffness. Solving for K in Eq. (15) we get $K=Z_o^2/M$, which we call the *matched-impedance condition*. To calculate the IM joint stiffness, we assume that the local characteristic impedance at the malleus is $Z_{ot}A_{tm}^2N_{rl}^2$, which is the characteristic impedance of the ear canal transformed to the IM joint.

Applying the matched-impedance condition, the IM joint stiffness K_{imj} is therefore

$$K_{imj}=\alpha_{im}\frac{(Z_{ot}A_{tm}^2N_{lr}^2)^2}{M_mN_{lr}^2}, \tag{16}$$

where the quantity in the parentheses is the local characteristic impedance at the malleus. The denominator is the malleus mass transferred to the other side of the transformer, with N_{lr} representing the lever ratio. We define the constant α_{im} as an impedance mismatch parameter between $\sqrt{K_{imj}M_m}$ and the local characteristic impedance. Based on direct observations of the cat IM joint slippage (Guinan and Peake, 1967), we have set $\alpha_{im}=\frac{2}{3}$. While the total number of parameters for the IM joint is two, the number of search parameters is one because of the estimate of α_{im}.

How does the matched impedance constrain help? If the ossicles were not matched, energy would be less effectively coupled to the cochlea, and the coupling would depend on frequency. Since wideband frequency measures of the cochlea (such as the cochlear microphonic, middle-ear pressure gain, and threshold of hearing) do not vary significantly with

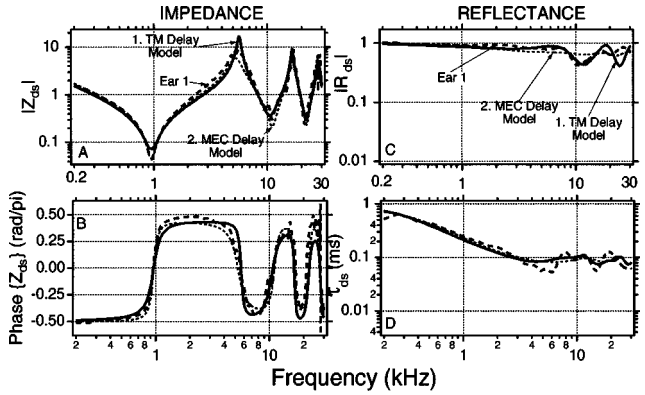

FIG. 6. Two model calculations are shown for the disarticulated stapes case, along with the measured data for ear 1: (1) The TM-delay model, and (2) the MEC-delay model. (A) Ear-canal impedance magnitude. (B) Impedance phase angle. (C) Reflectance magnitude. (D) The reflectance group delay $\tau(\omega)$.

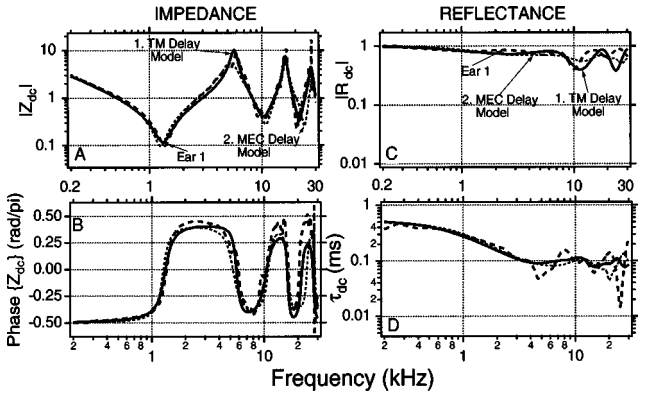

FIG. 7. Measurements (ear 1) and model calculation for the drained cochlea case. The complexity of this case increased from the disarticulated stapes case by the addition of the incudo–stapedial joint, the footplate area transformer, the annular ligament, and the stapes mass. These elements have an effect on the impedance and reflectance mostly at frequencies below 4–5 kHz. Above 4–5 kHz, the drained cochlea and the disarticulated stapes impedances and reflectances are approximately the same for both model calculations. (See Fig. 6 for a description of panels.)

frequency above a few kHz, we believe that the middle ear effectively couples ear-canal energy to the cochlea, justifying our assumption that $\alpha_{\rm im}=\frac{2}{3}$.

C. Disarticulated stapes

Because the stapes and cochlea have been removed, the disarticulated stapes case has the fewest number of parameters of the three conditions shown in Fig. 1. Fitting the TM and ossicle model requires the estimation of eight unknown parameters: the radiation load (2), the TM delay $T_{\rm tm}$ (1), the malleus stiffness $K_{\rm m}$, mass $M_{\rm m}$ and damping $R_{\rm m}$ (3), the IM joint damping $R_{\rm imj}$ (1), and the incus mass $M_{\rm i}$ (1).

An automatic search procedure was used that minimizes the error [see Eq. (A3)] between the measured impedance log magnitude and phase angle and model impedance log magnitude and phase angle. Starting from an initial estimate, the algorithm minimizes the error while searching a constrained parameter space (typically within 0.005 to 200 times the starting values) using a quasi-Newton algorithm. Several random perturbations by 25% of the initial parameters lead to the same solution.

Using this search procedure, the tympanic membrane delay model parameters were estimated for all three ears. The final parameters for ear 1 are listed in Table AI of the Appendix. Parameters for the other two ears typically differed from model parameters for ear 1 by less than a factor of 2. The TM delay in the other two ears was found to be approximately 34 μs for ear 2 and 41 μs for ear 3. Rather than list the parameters for the other two ears, we show the sensitivity of the TM-delay model to changes in model parameters in Fig. A1 of the Appendix.

The model and measured impedances for ear 1 for the disarticulated stapes case are shown in Fig. 6(A) and (B), while the reflectance magnitude and group delay are shown in Fig. 6(C) and (D). Both the TM-delay and MEC-delay models account for the high-Q standing waves.

Although the measured group delay at frequencies above 3 kHz has a mean value of approximately 100 μs, there is tendency for the delay of ear 1 to ''oscillate'' in frequency. The TM-delay model shows a similar oscillation. These correlated variations seem to be due to the acoustical properties of the middle ear. By removing the radiation load $Z_{\rm rl}$ in the model, we determined that $\tau_{\rm ds}(\omega)$ is a monotonically decreasing smooth function, *suggesting that the small oscillations above 6 kHz may be due to the radiation load impedance $Z_{\rm rl}$ causing a small impedance miss-match* (see also Fig. A1).

Figure 6 shows that, for the entire range of frequencies tested, *both* models are in agreement with measurements. We conclude that on the restricted evidence of impedance or reflectance, the delay can be either in the tympanic membrane or in the middle-ear cavity.

D. Drained cochlea

In going from the disarticulated stapes case to the drained cochlea case, model complexity increases by the addition of the incudo-stapedial joint, stapes mass $M_{\rm s}$, and annular ligament impedance. Four additional values for parameters $R_{\rm isj}$, $K_{\rm al}$, $R_{\rm al}$, and $M_{\rm s}$ are required for this case. Theoretical considerations suggest that the input impedance of the drained cochlea $Z_{\rm c_o}$ is negligible[6] in comparison with damping of the annular ligament $R_{\rm al}$ [Puria and Allen, 1991, Eq. (6a)].

As in the IM joint case, we apply the matched-impedance condition to the incudo-stapedial joint, treating the joint stiffness $K_{\rm isj}$ and the incus mass $M_{\rm i}$ as a segment of a parametric matched transmission line. The equation for the impedance-matched joint stiffness in terms of the mass and the local characteristic impedance is

$$K_{\rm isj}=\frac{(Z_{\rm ot}A_{\rm tm}^2N_{\rm lr}^2)^2}{M_{\rm i}}, \tag{17}$$

where the quantity in the parentheses is the local characteristic impedance at the incus.

The four additional parameters were obtained by manually adjusting them to obtain agreement between model and measured impedance magnitudes and phases, and are listed in Table AI. During this adjustment the parameters found for

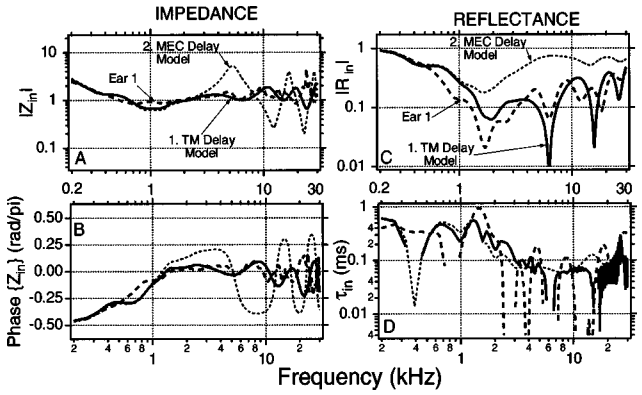

FIG. 8. Measurements (ear 1) and model calculations for the intact case. The complexity of this case is increased from that of the drained cochlea case by the addition of the cochlear load. The input impedance of a tapered cochlea with viscous perilymph was used as the cochlear load (Puria and Allen, 1991). (Note the change in scales of $|Z|$ and $|R|$ from previous figures.)

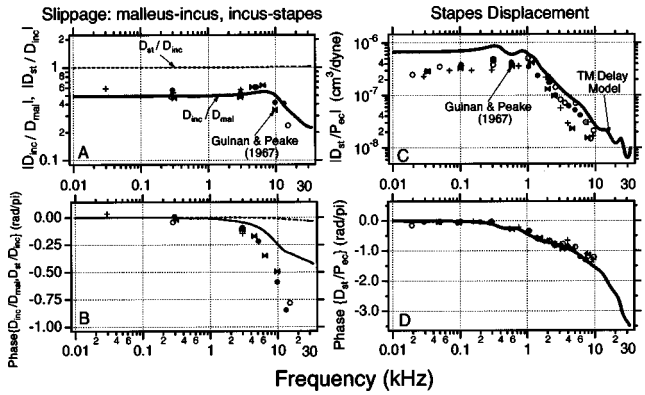

FIG. 9. Comparison of model calculations to measured data of the motions of the ossicles. Magnitude (A) and phase angle (B) of the slippage at the incudo-malleolar joint $D_{\text{incus}}/D_{\text{malleus}}$ and slippage at the incudo-stapedial joint $D_{\text{stapes}}/D_{\text{incus}}$. Magnitude (C) and phase angle (D) of the ratio of the stapes displacement in cm per dyn/cm^2 (74 dB SPL). The stapes volume-velocity $U_{\text{st}}(\omega)$ of the model was divided by $j\omega$ and the footplate area A_{fp} to obtain the stapes displacement D_{st}. Measurements by Guinan and Peake (1967) in four cat ears are shown as different symbols.

the disarticulated stapes case *were held fixed*. The estimated parameters for the stapes and annular ligament were found to be within a factor of 2 of those obtained experimentally by Lynch *et al.*, (1982). The average footplate area A_{fp} is known from anatomical measurements (Lynch *et al.*, 1982).

Model and measured impedances for ear 1, for the drained cochlea case, are shown in Fig. 7(A) and (B) and the reflectance magnitude and group delay are shown in Fig. 7(C) and (D). As may be seen from the measurements and model calculations, adding the stapes and the annular ligament stiffness has a significant effect below 5 kHz.

As in the disarticulated stapes case, Fig. 7 shows that both model results are consistent with measurements for a wide range of frequencies. *We conclude that, if one is given only impedance (or reflectance) measurements of the disarticulated stapes case or the drained cochlea case, it is impossible to determine the source of the delay.* We shall next show, however, that, once a cochlear load is attached (the ''intact ear'' case), the two hypothesis may be distinguished.

E. Intact ear

In going from the drained cochlea to the intact ear, the model complexity increases by the addition of the cochlear load impedance $Z_{\text{c}}(\omega)$ on the middle ear. As previously mentioned, our 1991 model of the cochlear input impedance, with tapered scalae area cochlea and viscous perilymph (Puria and Allen, 1991, Fig. 18), was used as the model cochlear load.

The parameters for both ME models were held fixed, and no new parameters were required for this calculation. The model and measured impedance magnitude and phase for the intact case of ear 1 is shown in Fig. 8(A) and (B), while the reflectance magnitude and group delay is shown in Fig. 8(C) and (D). With the cochlear load the impedance magnitude for ear 1 varies by about ± 6 dB. Consistent with previous results (Møller, 1965; Lynch, 1981; Allen, 1986), Fig. 8 shows that the cochlear load has a dramatic effect on the middle-ear impedance (and thus its reflectance).

For the TM-delay model, the standing waves in the impedance magnitude are significantly reduced, in comparison to the drained cochlea and the disarticulated stapes cases (Figs. 7 and 6). However, for the MEC-delay model, the impedance magnitude varies by as much as ± 15 dB, indicating standing waves that are much larger than in the TM-delay model. We conclude that the TM-delay model is consistent with measurements, while the MEC–delay model is inconsistent. Thus, *the middle-ear cavity delay hypothesis is ruled out.*

V. FURTHER TESTS OF THE TM-DELAY MODEL

An important test of any good model is that it can predict measurements not explicitly used in its formulation. In this section *generalizability* of the middle-ear model with TM delay is verified by comparing our model calculations with known physiological measurements from the literature.

We compare model results for the following middle-ear measurements from the literature: (1) incudo-malleolar and incudo-stapedial joint slippage, (2) the stapes displacement to ear-canal pressure ratio, and (3) the middle-ear pressure gain. These measurements were not used in the model formulation, with the exception of the IM joint slippage data.

A. Ossicular motion

1. Slippage of the ossicles

The ratio of the incus to malleus displacement ($D_{\text{inc}}/D_{\text{mal}}$ solid line) from the model is shown in Fig. 9(A) and (B) along with data points measured by Guinan and Peak (1967). Measurements and model magnitudes agree, while phase angles disagree by more than 0.5 rad/π above 10 kHz. In Eq. (16) the IM joint stiffness, and thus the impedance of the IM joint, is directly proportional to α_{im}. Although not shown, decreasing α_{im} has the effect of increasing the joint slippage. As is apparent from Fig. 5(B), decreasing the IM joint impedance will result in an increase in the current through the IM joint shunt branch and thus a decrease in V_{inc}, corresponding to increased slippage. Changes in α_{im} by 50% have a large effect on the IM slippage.

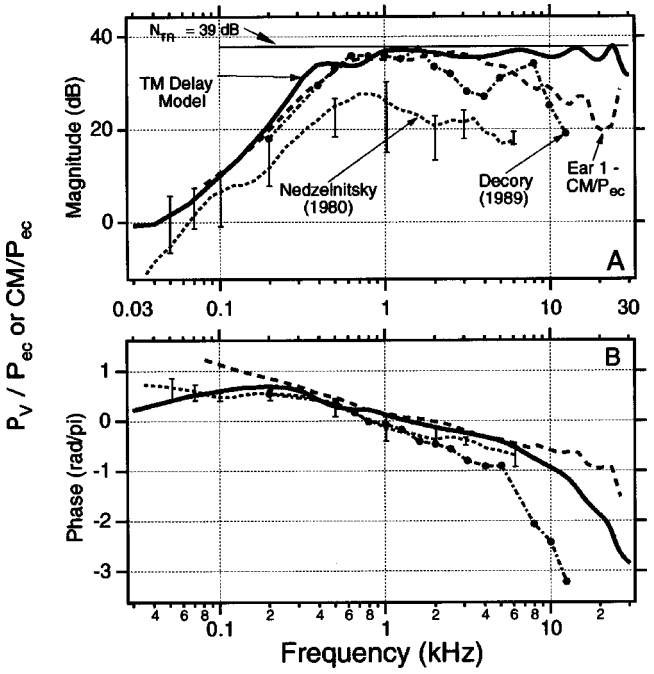

FIG. 10. Compared here are the middle-ear pressure gain of Nedzelnitsky and Décory, the ratio of the round window cochlear microphonic (CM) to the ear-canal pressure (P_{ec}) for ear 1, and model calculations of the middle-ear pressure gain. Two measurements of the middle-ear pressure gain with middle-ear cavities wide open are shown: (1) Nedzelnitsky's (1980) measurement is the median and range of six cats, and (2) Décory's (1989, Fig. 105) measurement is from one ear. Also shown is the CM data chosen from the linear regime of the CM (i.e., just before it started to saturate) and its magnitude scaled[7] (to agree with the pressure gain at 1 kHz) to allow comparison with the calculated middle-ear pressure gain. Panel A shows the magnitude in dB [$20\log_{10}(|X/P_{ec}|)$, where X is either P_v or CM] of the transfer function and panel B shows the phase angle in rad/π. The ''ideal mechanical transformer model'' is a zero-delay model that proposes that the product $(A_{tm}/A_{fp})\times N_{lr}$ is the pressure gain N_{TR} (Wever and Lawrence, 1950). For the cat, $N_{TR}\approx 39$ dB as shown by the straight line in panel A.

Our model calculations of the ratio of the incus to stapes displacement D_{inc}/D_{st}, as shown in Fig. 9(A) and (B), suggest that there is no significant slippage between these two ossicles even at the highest frequencies. This result is consistent with measurements of amplitude and phase between the incus and stapes displacement by Guinan and Peake (1967, pp. 1248–1249). Changes in K_{isj} by a factor of $\frac{1}{5}$ to 5 do not have a significant effect on the IS slippage because the stiffness of the IS joint is large. In order for there to be significant slippage in the IS joint, K_{isj} would need to be lower by a factor of 10 or more.

2. Stapes displacement

An important measure of middle-ear transmission is the ratio of the stapes displacement to the ear-canal pressure. The model computation of the stapes displacement (in cms) per unit of pressure at 1 dyn/cm^2 (74 dB SPL) is shown in Fig. 9(C) and (D). For comparison, the stapes displacement per unit ear-canal pressure data published by Guinan and Peak (1967) are also shown.

Below 500 Hz the model stapes displacement magnitude is greater than the measured values. For example, at 100 Hz the model results are greater by a factor of 2. At low frequencies, the stapes displacement is dominated by the malleus stiffness K_m (see Fig. A1) and the stiffness of the annular ligament K_{al}. Increases in K_m or K_{al} result in a decrease in stapes displacement, and this results in an increase in ear-canal impedance for frequencies below 1 kHz.

Lynch *et al.* (1994) established a correlation between body weight and eardrum compliance. One possible reason for the higher stapes displacement is that our animals (Fig. 1) had systematically lower stiffness than the Guinan and Peak animals (Fig. 9).

At high frequencies the phase shift in the stapes displacement re the ear-canal pressure [Fig. 9(D)] is much greater than the phase shift in the IM joint [Fig. 9(B)]. Thus the model IM joint does not account for most of the stapes displacement to ear-canal pressure phase shift. In the TM-delay model a portion of this phase is due to delay in the tympanic membrane.

B. ME pressure gain and round window cochlear microphonic

The *middle-ear pressure gain* is defined as the ratio of the vestibule pressure near the footplate to the ear-canal pressure near the tympanic membrane $P_v(\omega)/P_{ec}(\omega)$. This important ratio is related to the behavioral threshold (Puria *et al.*, 1997) and the cochlear microphonic (CM) response (Dallos, 1970; Nedzelnitsky, 1980; Allen, 1983).

As shown in Fig. 10 there is mixed agreement between the calculated middle-ear pressure gain and the measured pressure gain. In 1980 Nedzelnitsky (Fig. 15) reported measurements of the ME pressure gain in six cats with open ME cavity. In Fig. 10 these calculated and measured pressure gains are shown along with the measurements of cat middle-ear pressure gain from Décory (1989, Figs. 104–105), also for the wide open bulla condition. (Although not shown here, Décory also measured the pressure gain with an open bulla cavity but intact septum, and found the pressure to be lower than the mean of the removed septum by 3–6 dB.) Décory's measured pressure gain is greater than Nedzelnitsky's by 3–12 dB, while the phase angles are in reasonable agreement.

The middle-ear pressure gain was not measured for the ears used in the present study. However, the ratio of the round window cochlear microphonic[7] (CM) to ear-canal pressure was measured, and is labeled ''Ear 1-CM/P_{ec}'' in Fig. 10. It has been argued (Dallos, 1970; Allen, 1983), and is now widely accepted, that the CM is proportional to the pressure drop across the cochlear partition because, (a) the CM is proportional to basilar membrane displacement, (b) basilar membrane displacement is stiffness dominated for frequencies less than the characteristic frequency corresponding to the place of measurement, and (c) characteristic frequencies near the round window are greater than 30 kHz.

There is close agreement between the model calculations and both the pressure gain and the CM data in the 0.03–8-kHz frequency range (Fig. 10). Above 8 kHz, there are systematic differences in slopes of the magnitude of the round window CM and measured pressure gain and middle-ear model pressure gain. Above about 4 kHz the model slope is less than the CM slope by about 4 dB/oct.

VI. DISCUSSION

A. Testing the two hypotheses

The goal of the present work is to understand middle-ear mechanisms for frequencies above a few kHz. A reflectance group delay of approximately 100 μs has been found in the disarticulated stapes and drained cochlea cases for frequencies above 2 kHz [Figs. 6(D) and 7(D)]. Two hypotheses for the measured delay were tested: (1) the delay is in the tympanic membrane (TM-delay model), and (2) the delay is in the middle-ear cavity space (MEC-delay model). As shown in Fig. 5, we have assumed a series model for the ossicular chain and the middle-ear cavity space (Lynch, 1981, Chap. II; Puria, 1991b, pp. 133–135). We have quantitatively analyzed the two models.

Quantitative model calculations suggest that the two models are *not* distinguishable if one includes only the impedance for the disarticulated stapes and drained cochlea cases (Figs. 6 and 7). However, the two models are easily distinguished when the intact case is included, as seen in Fig. 8(A) and (B). The cochlear load significantly reduces the magnitude of the standing waves for the TM-delay model but not for the MEC-delay model. *All of the arguments above refute the middle-ear cavity delay hypothesis.*

1. The MEC-delay model

When the delay is in the middle-ear cavities, the resonances come from the standing waves in the MEC. In the MEC-delay model, the drum impedance is typically much smaller than the MEC impedance, namely $|Z_{oc}| \ll |Z_{mec}|$. For the intact case, the experimental TM impedance is approximately matched to the ear-canal characteristic impedance. This is inconsistent with the MEC-delay model because the large MEC impedance appears in series with Z_{oc}. In all three cases the impedance of the middle-ear cavity dominates at frequencies above 4–5 kHz and consequently changes in the ossicular chain impedance (i.e., due to draining the cochlea or disarticulating the stapes) do not have a significant effect on the ear-canal impedance at those frequencies.

2. The TM-delay model

When the delay is in the tympanic membrane, standing waves in the TM surface give rise to resonant modes. In this model the relative magnitude of Z_{mec} (due to the open middle-ear cavity) is small in comparison to Z_{oc}. Thus the ear-canal impedance Z_{ec} is dominated by Z_{oc}. The TM-delay model is sensitive to changes in the load to the ossicular chain, unlike the MEC-delay model.

B. Transmission line representation of the tympanic membrane

Once sound is collected by the external ear, it propagates into the ear canal where all higher-order modes below the ear-canal cutoff frequency are exponentially damped. Thus below approximately 25 kHz acoustic signals have a plane wave mode of propagation. Ideally, when this plane wave reaches the tympanic membrane 100% of the energy would be absorbed by the drum, and transferred to the cochlea. This could only happen if the TM had the same impedance as air, which it does not.

However, if at each point the stiffness were controlled, for example, by the TM curvature, then the annulus having the largest radius from the umbo would have the lowest stiffness, since its curvature there is smallest. If this stiffness were controlled in the proper way, the impedance of this outer annulus could have an impedance that is close to that of air. The wave speed on the TM would necessarily be lower, by the ratio of the density of air to the density of the TM. This would mean that the impinging plane wave would be absorbed in this portion of the TM with nearly zero reflection, and would be transformed into a transverse, slowly moving wave on the surface of the TM.

The resulting wave would then propagate into the umbo region along the radial axis. Due to the increasing TM curvature with radius, the local impedance of the transverse wave would increase. In this model of the TM, the main impedance transformation of the middle ear is in the TM itself, resulting from the propagation of the wave, and the gradient of the ear-drum stiffness. *This view of the acoustic surface wave on the eardrum is analogous to an acoustic horn having a radially dependent characteristic impedance.*

That portion of the ear-canal plane wave, incident on the umbo and manubrium, would be reflected, as this more central portion of the TM (unlike the annulus bounding the TM's circumference) would not match the impedance of air. Thus the reflectance, as measured in the ear canal, would depend on the percentage of the TM that is unmatched in specific acoustic impedance. This would set a low bound on the magnitude of the reflectance.

In this tympanic membrane with waves, the mass of the TM does not limit the performance of the system at high frequencies. The local TM mass is canceled by the local TM stiffness, forming a transmission line with delay. *Thus the distributed design trades mass for delay, giving the transfer function a much wider bandwidth than attainable with a lumped parameter model* (e.g., the two-piston model of the TM of Shaw or the one-piston TM model of Zwislocki).

Specifically, we represent the TM by a lossless transmission line, with a frequency independent delay of approximately 36 μs (for ear 1). This representation allows for the possibility of standing waves on the tympanic membrane.[8] Representing the TM as a lossless frequency-independent delay, as in Eq. (13), is only a first-order approximation, and one that is shown to be reasonable to fairly high frequencies. Recent measurements between 2 and 46 kHz provide further evidence that there is frequency-independent delay in the middle-ear system. Olson (1998) has shown that the phase of the gerbil middle-ear pressure gain is approximately linear with a corresponding delay of approximately 25 μs. Future measurements of the TM transmission matrix [Eq. (14)] will be the definitive tests of the model presented here.

In summary, the mechanics of the auditory periphery consists of a cascade of transmission lines. These are the concha, the ear canal, the tympanic membrane, the ossicles, and the organ of Corti.

1. Tympanic membrane wave speed

For a TM area of 0.41 cm^2 (Wever and Lawrence, 1954, p. 416) the radius is approximately 0.361 cm, and the corresponding wave speed, for a 35.7-μs delay, is approximately 10.1×10^3 cm/s. Such a wave speed on the TM is slower, by a factor of 3.4, than the speed of sound in air.

In our formulation for the TM [Eq. (13)], a small section of the TM corresponds to an annulus on the TM which has a local wave velocity approximated to be same regardless of the radial position. A refinement to this idea could be a model where the local wave velocity depends of the radial position along the TM; however, the motivation for such a model remains unclear.

2. Standing waves on the tympanic membrane

We have analyzed the transmission line representation for the TM from an input–output point of view. Another approach is to analyze the *spatial* response of the TM transmission line.

Given a unit ear-canal pressure, the ear-canal impedance is the reciprocal of the volume velocity. Cancellations of the volume velocities across the TM surface, due to portions of the TM moving with different phases, would result in a relatively small ear-canal volume velocity, and thus a relatively large middle-ear impedance magnitude. Conversely, when the entire TM surface moves in phase, the ear-canal volume velocity is relatively large, corresponding to a small middle-ear impedance magnitude.

Time-averaged holographic methods show that for frequencies above 3 kHz and levels greater than 90 dB SPL, the surface of the ''tympanic membrane vibrations break up into sections,'' suggesting that the TM is not a stiff plate (Khanna and Tonndorf, 1972). These measurements are consistent with our conclusions that there are standing waves on the TM. Thus, the Khanna and Tonndorf (1972) observation is consistent with our model that acoustic waves travel on the tympanic membrane.

It would be instructive to measure the tympanic membrane surface displacement patterns before and after removing the cochlear load from the middle ears of the same animals. Our model prediction is that the magnitude of the standing waves observed on the tympanic membrane surface should increase significantly after draining the cochlea, or after cutting the incudo-stapedial joint.

C. Two-port matrix representation

The most important difference between the current model and previous models is the representation of the tympanic membrane. Comparisons among various models for the TM can be facilitated by analyzing them in terms of a two-port transmission matrix representation. Such a characterization is interesting because two of the elements of the transmission matrix have a specific physical interpretation in terms of area (Shera and Zweig, 1991). The reciprocal of the matrix element $A_{\rm tm}(\omega)$ in Eq. (13) is the effective area $A_F(\omega)$ corresponding to the ratio of the ear-canal pressure and umbo force. Matrix element $D_{\rm tm}(\omega)$ is the effective area $A_V(\omega)$ corresponding to the ratio of the ear-canal volume velocity and umbo velocity. For a piston (ridged plate) model of the TM, the magnitude of the A_F to A_V ratio is by definition unity and deviations from unity indicate the degree to which a particular TM model deviates from a plate model.

In our two-port formulation for the TM model [Eqs. (13) and (14)] A_F is $A_{\rm tm}/\cos(\omega T_{\rm tm})$ and A_V is $A_{\rm tm}\cos(\omega T_{\rm tm})$. Thus the ratio of the areas is simply

$$\frac{A_F}{A_V}=\frac{1}{\cos^2(\omega T_{\rm tm})}. \tag{18}$$

This equation states that in the present model the ratio of the areas clearly does not behave like a piston and, furthermore, the area ratio is a periodic function of frequency. The first peak in the area ratio occurs when $\omega T_{\rm tm}=\pi/2$, or at a frequency of $(4T_{\rm tm})^{-1}$. For a TM delay of 35.7 μs this corresponds to a frequency of 7 kHz, and thus the maxima and minima in Eq. (18) occur at multiples of 7 kHz. Further measurements of the transmission matrix elements [Eq. (14)] are needed to verify Eq. (18).

D. Previous tympanic membrane models

1. Lumped parameter representations

Matthews (1983) represented the cat TM with a one-degree of freedom model, consisting of a series resistor, mass, and stiffness. He showed that the model input impedance diverges from the measured data for frequencies above 3–4 kHz. The problem is that the model impedance is mass dominated above 4 kHz, whereas the measurements are approximately resistive. As discussed by Matthews (1983), the failure is primarily due to an inadequate representation of the tympanic membrane.

A natural extension of the one–degree of freedom TM piston model is the two–degrees of freedom model. We have previously attempted to model the data of Fig. 1 with such a model (Puria, 1991b; Puria and Allen, 1994). However, that model proved unsatisfactory because the parameters depended on the measurement condition, which is nonphysical.

Another two-degrees of freedom model is the ''two-piston model'' for the human TM (Shaw, 1977; Shaw and Stinson, 1981, 1983; Goode *et al.*, 1994). The two-piston model has been tested only for frequencies up to approximately 8 kHz (Shaw and Stinson, 1981). To evaluate delays in the most recent incarnation of the two-piston model we have calculated the reflectance group delay in the Goode *et al.* (1994) model. Above 5 kHz the group delay is less than 30 μs in contrast to the approximately 100 μs measured in the cat ear (Fig. 3). Thus the two-piston model with parameters for the human ear does not appear to have the required delays for high frequencies and it therefore seems inconsistent with the cat middle-ear measurements. We feel the two-piston model needs further study.

2. Finite-element models

Most finite-element models of the middle ear have only been tested at low frequencies (Funnell and Laszlo, 1978; Funnell, 1983; Wada *et al.*, 1992). Very interesting is the work of Funnell *et al.* (1987) in which the magnitude of the umbo displacement, and points anterior and posterior, were

reported for frequencies up to 20 kHz. Their model calculations suggest that not all parts of the TM move with the same amplitude. However, the overall behavior of the TM is not evident from the calculations reported. It would be instructive to recompute the input impedance for the finite-element models for the conditions of Figs. 6 and 7. Wada *et al.* (1992) have made such calculations, but only for frequencies below 2 kHz. Other important measures, such as the middle-ear pressure gain, should also be calculated by loading the finite-element model with a cochlear load. One undesirable aspect of finite-element models is the large number of parameters that need to be estimated. The present finding of TM-delay imposes important model constraints and thus incorporating TM delay can help to greatly reduce the number of parameters in the finite-element models.

E. Mass of the ossicles

We next ask: Are the parameters for the mass of the ossicles used in the model reasonable? We chose these values by a global parameter search under the constraint that the ossicles form a matched segment of discrete transmission line. Lynch (1981, p. 236) measured the malleus mass to be 11.134 ± 0.627 mg, while the incus mass was 4.313 ± 0.328 mg. The malleus mass used in TM-delay models may be estimated from

$$M_{\mathrm{m}} = \frac{M_{\mathrm{m}}^{w} \kappa^2}{L_{\mathrm{m}}^2}, \tag{19}$$

where M_{m}^{w} is the measured mass of the malleus, κ is the radius of gyration, and L_{m} is the length of the malleus. The numerator in Eq. (19) corresponds to the moment of inertia of the malleus. If one uses Lynch's (1981, pp. 231–233) estimate of 0.15 cm for κ, 0.4 cm for L_{m} (Wever and Lawrence, 1954), and $M_{\mathrm{m}} = 0.37$ mg (Table AI), then the model M_{m}^{w} is 2.6 mg, which is a factor of 4.2 smaller than Lynch's average malleus mass. This factor might be accounted for by the smaller size animals used in the present study in comparison to those of Lynch *et al.* (1994). Another explanation might be differences in the radius of gyration between Lynch's measurements and those in the present study.

Lumped-parameter models typically have mass element values that are significantly greater than measured values. Examples 1 and 2 in Fig. 4(C) indicate that at low frequencies the lumped-parameter model is indistinguishable from models that have added delay (since they are both stiffness dominated). The higher frequency resonances are apparent due to the added delay [Fig. 4(C), examples 2 and 3]. The resonances appear as a quasi-periodic series of mass and stiffness dominated regions. In the past, modelers have used inductors and capacitors to represent mass and stiffness regions (e.g., Matthews, 1983; Kringlebotn, 1988; Puria, 1991; Puria and Allen, 1994). For instance, in Fig. 4(C) example 2, the impedance is masslike in the 2- to 6-kHz region. To account for this masslike impedance one could add a mass term to K_{m} to obtain a reasonable fit for frequencies below 6 kHz. However, this would result in a model that works only for frequencies below 6 kHz. In addition, this mass term needs to be fairly large in comparison with measured mass of the ossicles. It is perhaps for these reasons that estimates of the malleus mass in previous middle-ear models (Peake and Guinan, 1967; Matthews, 1983; Puria, 1991b) have been approximately an order of magnitude greater[9] than the mass estimated by the model with TM delay (Table AI). Thus in the model of Fig. 5(B), *mass has been traded for delay resulting in a middle-ear input impedance which is, consistent with experiments, not mass dominated at high frequencies* [Fig. 8(A) and (B)].

F. Pressure reflectance to power

Transforming the impedance to the reflectance domain allows for a much simpler description of a distributed system; the relative power transfer from a source to a load is equal to $1-|R|^2$ (Carlin and Giordano, 1964; Siebert, 1970; Puria, 1991b; Voss and Allen, 1994), while the poles and zeros are described by the phase of R [Eq. (11)].

For the disarticulated stapes case almost all the energy is returned; the reflectance magnitude is between 0.8 and 1.0 for frequencies below 8 kHz. This means that the drum and ossicles are largely reactive, with a relative power absorption that is on the average less than $1-0.9^2 \approx 0.20$, or 20%. The TM is loaded by the stiffness of the malleus ligament and the stiffness of the incudo-malleolar joint. Losses seen in these measurements are probably due to damping in the ligaments and, at higher frequencies, to losses in the radiation load impedance.

For the drained cochlea, $1-0.8^2$ or 36% of the power is absorbed in the mid-frequency range. This implies that, to a first-order approximation, $36\%-20\%=16\%$ of the energy may be absorbed by the annular ligament in this frequency range.

For the intact case, and in the 1–6-kHz region, the pressure reflectance is less than 0.2. This means that $1-0.2^2 = 0.96$ is the fraction of the power absorbed. We conclude that more than $96\%-36\% \approx 60\%$ of the power is absorbed by the cochlea.

G. Middle-ear pressure gain

In Fig. 10 the middle-ear pressure gain from the model is compared to measurements of the middle-ear pressure gain and of the round-window CM to ear-canal pressure ratio ($\mathrm{CM}/P_{\mathrm{ec}}$). For frequencies below approximately 8 kHz, the middle-ear pressure gain in the model is similar to the measured pressure gain, and has similar frequency dependence to $\mathrm{CM}/P_{\mathrm{ec}}$. However, the model gain is typically higher than both measurements for frequencies above 8 kHz. Possible reasons include: (1) nonpistonlike stapes motion or (2) inadequate representation of the cochlear load.

Dallos (1974) has noted that the magnitude of the CM transfer function, recorded with differential electrodes, and the magnitude of the scala-vestibule pressure (Nedzelnitsky, 1974), are in good agreement for the 20-Hz to 2-kHz range. Our observations extend in frequency Dallos' observation.

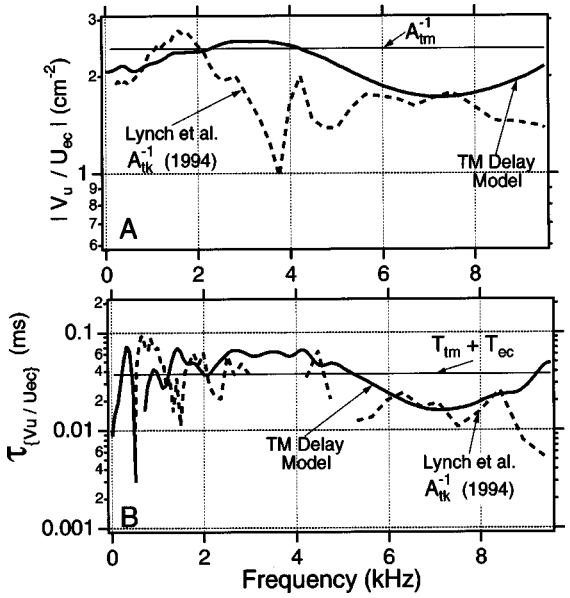

FIG. 11. Umbo-velocity to ear-canal volume–velocity ratio $V_u(\omega)/U_{ec}(\omega)$ in the ''TM-delay model'' is compared with A_{tk}^{-1} the reciprocal of the kinematic area reported by Lynch *et al.* (1994). (A) The magnitude of V_u/U_{ec}. The reciprocal of the area of the TM is labeled A_{tm}^{-1}. (B) The group delay calculated from the phase of V_u/U_{ec}. The sum of the delay in the TM transmission line T_{tm} and the delay in the residual ear-canal space T_{ec} is labeled $T_{tm}+T_{ec}$. For both the model calculations and the data, negative group delays have been omitted from the plot.

H. Umbo-velocity to ear-canal volume–velocity ratio

Another test of the tympanic membrane acoustic delay hypothesis is the umbo velocity V_u to the ear-canal volume-velocity U_{ec} ratio (V_u/U_{ec}), which can be expressed as the product of two measurable functions: (1) the umbo velocity to ear-canal pressure ratio, and (2) the middle-ear input impedance Z_{ec}. Namely

$$\frac{V_u}{U_{ec}} = \frac{V_u}{P_{ec}} Z_{me}, \tag{20}$$

which has dimensions of an inverse area (cm^{-2}) and is the reciprocal of the effective area of the tympanic membrane (e.g., Wever and Lawrence, 1954, Chap. 6,7; Møller, 1983, pp. 25–30).

The two measurements (V_u/P_{ec} and Z_{me}) have not been made in the same animals with the middle-ear cavities wide open. However, the product of the two measurements was reported by Lynch *et al.* (1994). In the Lynch *et al.* terminology, V_u/U_{ec} is the reciprocal of the kinematic area $1/A_{tk}$ of the tympanic membrane. For a piston model of the tympanic membrane A_{tk}^{-1} is A_{tm}^{-1}. Figure 11 shows V_u/U_{ec} for the TM-delay model and $1/A_{tk}$ from measurements. Not surprisingly, there are differences in the model and measurements in the 2–5-kHz region due to closed middle-ear cavity for the measurements. However, the measured group delay of $1/A_{tk}$ and model group delay of V_u/U_{ec} are consistent with our TM delay hypothesis. Measurements of V_u/U_{ec} from the same animals, with open MECs and at higher frequencies, are needed.

VII. SUMMARY

The present study reveals the presence of tympanic membrane acoustic delay in physiological measurements of the cat middle ear. The simplified TM-delay model presented here allows us to address one of the basic issues of the physical properties of the ear drum: *Is the tympanic membrane acting as a combination of stiffness and mass terms (lumped-element system), or does it act as a transmission line (distributed system)?* We conclude that to a first-order approximation the tympanic membrane may be represented as lossless transmission line with frequency-independent delay. Our model of a tympanic membrane delay structure, and the assumption of a matched impedance condition for the ossicles, allows effective coupling of sound to the inner ear over a much higher frequency range than would be otherwise possible.

The tympanic membrane delay model is used in a comprehensive middle-ear model [Fig. 5(B)] that describes a wide range of measurements, namely:

—middle-ear impedance and reflectance for the disarticulated stapes, drained cochlea, intact ossicles and cochlea,
—stapes displacement to ear-canal pressure ratio,
—middle-ear pressure transfer function,
—umbo velocity to ear-canal volume–velocity ratio.
—incudo-malleolar joint slippage, and
—incudo-stapedial joint slippage.

All the model calculations to 25 kHz use a single set of parameters. Above a few kHz, measurements and model calculations critically depend on our hypothesis that tympanic membrane acoustic delay is large in comparison with delay in other middle-ear structures.

ACKNOWLEDGMENTS

We thank Paul Fahey, Patricia Jeng, Douglas H. Keefe, William T. Peake, John J. Rosowski, Christopher A. Shera, M. Mohan Sondhi, Neshie Tiwari, Arnold Tubis, and Susan Voss. They have helped shape this manuscript over the past few years. We specially thank J. Tonndorf who was our

TABLE AI. Estimated parameters for the cat middle-ear model of Fig. 5(B). The form of the first seven functions (Z_m to Z_{rw}) is $Z=R+K/j\omega+j\omega M$. The units for mechanical impedances, denoted by superscript ''*m*'' in column 2, are: *R* (dyne-s/cm), *K* (dyn/cm), and *M* (g). The units for acoustical impedances, denoted by superscript ''*a*'' in column 2, are: *R* (dyne-s/cm^5), *K* (dyn/cm^5), and *M* (g/cm^4). The radiation load impedance of the vented middle-ear cavity is given by Eq. (12).

Description	Symbol	*R*	*K*	*M*
Malleus	Z_m^m	4	1.5×10^5	3.7×10^{-4}
IM joint	Z_{imj}^m	1	3.3×10^7	0
Incus	Z_i^m	0	0	1.1×10^{-4}
IS joint	Z_{isj}^m	10	6.6×10^8	0
Annular ligament	Z_{al}^a	1×10^5	5.3×10^9	0
Stapes	Z_s^a	0	0	3.3
Round window	Z_{rw}^a	0	1.2×10^8	0
Radiation load	Z_{rl}^a	160	⋯	5.6×10^{-3}
Eardrum delay	$T_{tm}=35.72\ \mu s$			

teacher and colleague. Many of our experimental techniques regarding the modifications to the ear were developed under his guidance. Support for author SP came in part from Grant Nos. F32 DC00073, R03 DC02677, PO1 DC00119, and R29 DC03085 of the National Institute on Deafness & Other Communication Disorders of the National Institutes of Health.

APPENDIX: MODEL PARAMETERS AND SENSITIVITY ANALYSIS

A. Tympanic membrane delay model parameters

The middle-ear parameters for the tympanic membrane delay model of Fig. 5(B) were first estimated for the simplest case of the disarticulated stapes. An automatic search algorithm was used to estimate the parameters from the measured impedance Z_{ds} for this case. Additional parameters were then estimated for the case of the drained cochlea, while holding the established parameters fixed. Finally, calculations were made for the intact case by loading the drained cochlea model with a cochlear load (Puria and Allen, 1991). In all cases, once each parameter was established, it was not allowed to change for the next more complex case. The parameters used in this model are shown in Table AI.

B. Sensitivity analysis of the TM-delay model

The sensitivity of the tympanic membrane delay model to parameter changes was estimated by computing the ear-canal impedance and reflectance before and again after increasing and decreasing each parameter by a factor of 3. Calculations for six of the eight parameters used in the minimization procedure, for the disarticulated stapes case, are shown in Fig. A1. The incus mass (M_i) has a sensitivity similar to that of M_m, while Z_{ds} is insensitive to changes in R_{jim} and thus are not shown.

To quantify the effect of changes in model parameters we estimate the rms error in both the log magnitude and

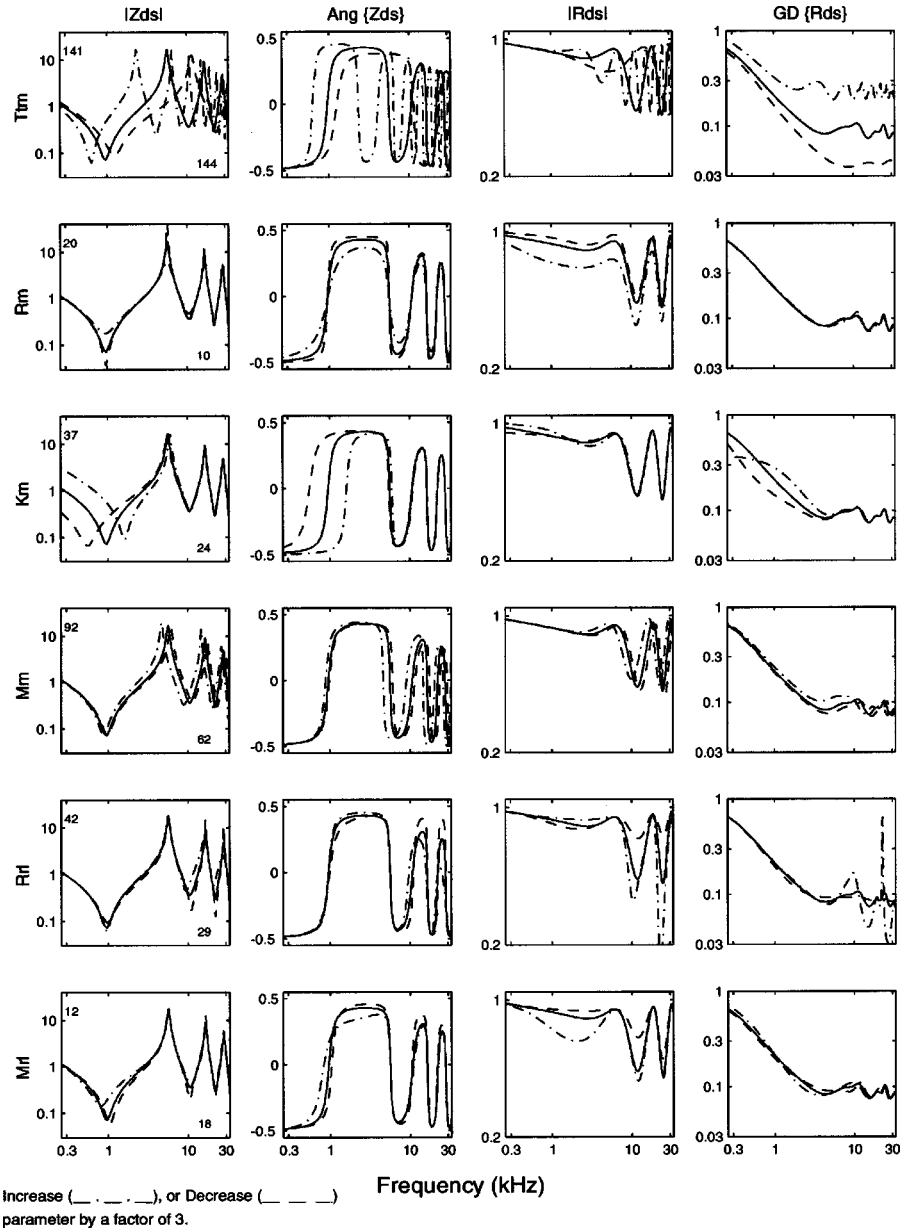

FIG. A1. Sensitivity of the tympanic membrane delay model (disarticulated stapes case) to a parameter increase and decrease by a factor of 3. In all plots, the solid line indicates the model calculated with parameters from Table AI. Model computations with the increased parameter are plotted with a dash–dot line (–·–·–), while calculations with the decreased parameter are plotted with a dashed line (– – –). The first and second columns show the normalized impedance magnitude and angle (rad/π), while the third and fourth columns show the (dimensionless) reflectance magnitude and group delay (ms). The frequency range is from 300 Hz to 30 kHz. The parameter varied for a given row is indicated on the left side of the row. For example, in row 1 the tympanic membrane delay T_{tm} is varied. The total error in the impedance magnitude and phase [Eq. (A3)], due a variation in parameter, is indicated in each plot of column one (labeled $|Z_{ds}|$). The number on the upper-left side indicates the error due to an increase in the respective parameter, while the number on the lower-right side indicates the error due to a decrease in the respective parameter.

TABLE AII. Parameters estimated for the middle-ear cavity delay model [Fig. 5(B) and (C)]. The form of the functions is described in Table AI.

Description	Symbol	R	K	M
Malleus	Z_m^m	5×10^{-11}	1.7×10^{5}	3.2×10^{-5}
IM joint	Z_{imj}^m	1	3.9×10^{8}	0
Incus	Z_i^m	0	0	3.1×10^{-2}
Radiation load	Z_{rl}^a	90.4	⋯	6.4×10^{-3}
Middle-ear cavity	$L_{mec}=1.4$ cm			
	$D_{mec}=0.35$ cm			

phase of the impedance as a function of model parameters. The rms error in the log impedance magnitude domain is

$$\varepsilon_m=\sqrt{\frac{1}{N_f}\sum_{i=1}^{N_f}\{100[\log_{10}|Z_{\text{ds}}(\omega_i)|-\log_{10}|\overline{Z}_{\text{ds}}(\omega_i)|]\}^2}. \tag{A1}$$

The rms error in the phase of the impedance is

$$\varepsilon_p=\sqrt{\frac{1}{N_f}\sum_{i=1}^{N_f}[\angle Z_{\text{ds}}(\omega_i)-\angle\overline{Z}_{\text{ds}}(\omega_i)]^2}, \tag{A2}$$

where the impedance angle is in degrees.

The total error in the impedance domain is

$$\varepsilon_z=\varepsilon_p+\varepsilon_m. \tag{A3}$$

In the above equations Z_{ds} is the model impedance with normal parameters (Table AI) and $\overline{Z}_{\text{ds}}$ is for the model impedance with modified parameters. The factor of 100 in Eq. (A1) introduces a weighting factor that gives approximately equal weights to the magnitude and phase of the error in Eq. (A3). The error function ε_z was evaluated on a log-frequency axis. The minimization procedure used to estimate the middle-ear model parameters depended on the error function described by Eq. (A3).

In Fig. A1, ε_z due to an increase in the parameter is indicated in the upper left corner, while ε_z due to a decrease in the parameter is indicated in the lower right corner of the first column. For reference, if $|\overline{Z}_{\text{ds}}|=1$ and $\angle\overline{Z}_{\text{ds}}=0$, then ε_z is just a little more than 100. Figure A1 shows that the TM-delay model is most sensitive to the TM-delay T_{tm} and the malleus mass M_{m}. This is primarily because both T_{tm} and M_{m} have a broadband effect on the ear-canal impedance, whereas the other parameters have their greatest effect either at low frequencies (R_{m},K_{m},M_{rl}), or at high frequencies (R_{rl}).

For the drained cochlea case, the sensitivity of the model to changes in K_{al} and R_{al} is similar to changes in K_{m} and R_{m}, respectively.

C. Middle-ear cavity model parameters

As in the TM-delay model, the parameters for the middle-ear cavity model [Fig. 5(B) and (C)] were also estimated for the disarticulated stapes case using the same methods described above. The optimum parameters found for the disarticulated stapes case are listed in Table AII. A sensitivity analysis (like that shown in Fig. A1) shows that a perturbation (by a factor of 2–3) of the parameters listed in Table AII resulted in a significant change in ear-canal impedance. Parameter R_{m}, required a much a significantly larger perturbation.

Another important parameter is the length of the middle-ear cavity L_{mec} because the delay in the middle-ear cavity is a function of this length. Here L_{mec} was estimated to be 1.4 cm by the search procedure. Although the dimensions of the tympanic cavity and the bulla cavity are irregular, this length estimate is consistent with reported dimensions of the cat middle ear cavities (Huang *et al.*, 1997). Based on this length, and volumetric measurements of middle-ear space of the cat (Huang *et al.*, 1997), the effective diameter the cat middle-ear cavity D_{mec} should be approximately 0.9 cm. A diameter of 0.35 cm, found by the minimization procedure, is much smaller than the expected value.

[1]The four-load calibration method requires that the impedances of the four loads be different at all frequencies by carefully choosing the lengths of the four calibration cavities (Allen, 1986; Voss and Allen, 1994). The lengths of the cavities used for the measurements reported here were such that the impedances of the four cavities were very close to each other in the 15–16-kHz frequency region. As a result calibration errors are larger in that frequency region.

[2]Ear 1, ear 2, and ear 3 here correspond to C82-L, C88-L, and C88-R, respectively.

[3]Measurements on ear 1 were previously reported (Allen, 1986). We choose this ear based on several criteria, designed to select the pristine ear. The best predictor we have found of the undamaged ear is a visually transparent TM (Stinson and Khanna, 1994).

[4]The tenth-order filter coefficients were truncated to a length of 65 in the time domain.

[5]Although not shown here, a few impedance measurements made after removing the TM confirm that the functional form of Eq. (12) is approximately correct.

[6]When drained, air replaces the perilymph of the inner ear. The characteristic impedance of the cochlea at the stapes is

$$Z_{c_0}=\sqrt{\frac{4\rho_0K_0'}{S_0}},$$

given the assumption that viscous and thermal effects are insignificant when the cochlea is air filled. Using $\rho_0=1.18\times10^{-3}$ g/cm^3 for the density of air, $K_0'=1.7\times10^9$ dyn/cm^4 for the BM stiffness at the base, and $S_0=0.02$ cm^2 for the area at the base of the cochlea, we obtain $Z_{c_0}\approx2\times10^4$ dyn-s/cm^5. Lynch *et al.*'s (1982) experimental averaged value for R_{al} is 2×10^5; an order of magnitude greater than Z_{c_0}. Thus the impedance of the air filled cochlea represents an insignificant load to the stapes in the drained cochlea case [Puria and Allen, 1991, Eq. (6a)].

[7]The CM sensitivity at 1 kHz is about 1 mv/Pa (Allen, 1983). The CM magnitude was multiplied by 86 and then converted to dB.

[8]Zwislocki (1962, p. 1517) postulated that at high frequencies the motion of the TM could perhaps be represented by a transmission line.

[9]The acoustic mass of the malleus in three previous models of the cat middle ear are: 0.04 g/cm^4 (Matthews, 1983), 0.022 g/cm^4 (Peake and Guinan, 1967), and 0.013 g/cm^4 (Puria, 1991b). The mechanical mass of malleus transformed to the ear canal side of the TM, where it can be measured, is referred to as the acoustic mass. The relationship between acoustical mass and mechanical mass is: $M_a^m=A_{\text{tm}}^2M_m^a$. For a TM area of 0.41 cm^2 (Table AI) the mechanical mass for the three models is 6.7, 3.7, and 2.2 mg, respectively.

Allen, J. B. (**1983**). ''Magnitude and phase-frequency response to single tones in the auditory nerve,'' J. Acoust. Soc. Am. **73(6)**, 2071–2092.

Allen, J. B. (**1986**). ''Measurement of eardrum acoustic impedance,'' in *Peripheral Auditory Mechanisms*, edited by J. B. Allen, J. L. Hall, A. Hubbard, S. T. Neely, and A. Tubis (Springer-Verlag, New York), pp. 44–51.

Békésy, G. (**1960**). *Experiments in Hearing* (McGraw-Hill, New York).

Beranek, L. L. (**1954**). *Acoustics* (McGraw-Hill, New York).

Carlin, H. J., and Giordano, A. B. (**1964**). *Network Theory—An Introduction to Reciprocal and Nonreciprocal Circuits* (Prentice-Hall, Englewood Cliffs, NJ).
Dallos, P. (**1970**). ''Low-frequency auditory characteristics: Species dependence,'' J. Acoust. Soc. Am. **48**, 489–499.
Dallos, P. (**1974**). ''Comments,'' in *Facts and Models in Hearing*, edited by E. Zwicker and E. Terhardt (Springer-Verlag, New York), p. 54.
Décory, L. (**1989**). ''Origins of interspecific differences in susceptibility to noise,'' Ph.D. thesis, The University of Bordeaux II.
Flanagan, J. L. (**1962**). ''Computational model for basilar-membrane displacement,'' J. Acoust. Soc. Am. **34**, 1370–1376.
Funnell, W. R. J. (**1983**). ''On the undamped natural frequencies and mode shapes of a finite-element model of the cat eardrum,'' J. Acoust. Soc. Am. **73**, 1657–1661.
Funnell, W. R. J., and Laszlo, C. A. (**1978**). ''Modeling of the cat eardrum as a thin shell using the finite-element method,'' J. Acoust. Soc. Am. **63**, 1461–1466.
Funnell, W. R. J., Decraemer, W. F., and Khanna, S. M. (**1987**). ''On the damped frequency response of a finite-element model of the cat eardrum,'' J. Acoust. Soc. Am. **81**, 1851–1859.
Giacoletto, L. J. (**1977**). *Electronic Designers' Handbook* (McGraw-Hill, New York), 2nd ed.
Goode, R., Killion, M., Nakamura, K., and Nishihara, S. (**1994**). ''New knowledge about the function of the human middle-ear: development of an improved analog model,'' Am. J. Otolaryngol. **15(2)**, 145–154.
Guinan, J., and Peake, W. T. (**1967**). ''Middle-ear characteristics of anesthetized cats,'' J. Acoust. Soc. Am. **41**, 1237–1261.
Huang, G. T., Rosowski, J. J., Flandermeyer, D. T., Lynch, T. J., III, and Peake, W. T. (**1997**). ''The middle ear of a lion: Comparison of structure and function to domestic cat,'' J. Acoust. Soc. Am. **101**, 1532–1549.
Keefe, D. H., Ling, R., and Bulen, J. C. (**1992**). ''Method to measure acoustic impedance and reflection coefficient,'' J. Acoust. Soc. Am. **91**, 470–485.
Keefe, D. H., Bulen, J. C., Arenhart, K. H., and Burns, E. M. (**1993**). ''Method to measure acoustic impedance and reflection coefficient,'' J. Acoust. Soc. Am. **94**, 2617–2638.
Khanna, S. M., and Tonndorf, J. (**1972**). ''Tympanic membrane vibrations in cats studied by time-averaged holography,'' J. Acoust. Soc. Am. **51**, 1904–1920.
Kringlebotn, M. (**1988**). ''Network model for the human middle ear,'' Scand. Audiol. **17**, 75–85. Lync
h, T. J. (**1981**). ''Signal processing by the cat middle ear: Admittance and transmission, measurements and models,'' Ph.D. thesis, MIT.
Lynch, T. J., Nedzelnitsky, V., and Peake, W. T. (**1982**). ''Input impedance of the cochlea in cat,'' J. Acoust. Soc. Am. **72**, 108–130.
Lynch, T. J., Peake, W. T., and Rosowski, J. J. (**1994**). ''Measurements of the acoustic input impedance of cat ears: 10 Hz to 20 kHz,'' J. Acoust. Soc. Am. **96**, 2184–2209.
Matthews, J. W. (**1983**). *Modeling Reverse Middle Ear Transmission of Acoustic Distortion Signals* (Delft U.P., Delft, The Netherlands), pp. 11–18.
Møller, A. R. (**1965**). ''An experimental study of the acoustic impedance of the middle ear and its transmission properties,'' Acta Oto-Laryngol. **60**, 129–149.
Møller, A. R. (**1983**). *Auditory Physiology* (Academic, New York).
Nedzelnitsky, V. (**1974**). ''Measurements of sound pressure in the cochleae of anesthetized cats,'' in *Facts and Models in Hearing*, edited by E. Zwicker and E. Terhardt (Springer Verlag, New York), pp. 45–53.
Nedzelnitsky, V. (**1980**). ''Sound pressures in the basal turn of the cat cochlea,'' J. Acoust. Soc. Am. **68**, 1676–1689.
Nuttall, A. L. (**1974**). ''Measurements of the guinea-pig middle-ear transfer characteristic,'' J. Acoust. Soc. Am. **56**, 1231–1238.
Olson, E. S. (**1998**). ''Observing middle and inner ear mechanics with novel intracochlear pressure sensors,'' J. Acoust. Soc. Am. **103**, 3445–3463.
Onchi, Y. (**1961**). ''Mechanism of the middle ear,'' J. Acoust. Soc. Am. **33**, 794–805.
Papoulis, A. (**1962**). *The Fourier Integral and its Applications* (McGraw–Hill, New York).
Peake, W., and Guinan, J. (**1967**). ''Circuit model for the cat's middle ear,'' MIT Research Laboratory of Electronics, Quarterly Prog. Rep. No. 84, 320–326.
Puria, S. (**1991a**). ''A physical model for the middle-ear cavity,'' J. Acoust. Soc. Am. **89**, 1864.
Puria, S. (**1991b**). A theory of cochlear input impedance and middle ear parameter estimation, Ph.D. thesis, The City College, CUNY.
Puria, S., and Allen, J. B. (**1989**). ''Impedance measurements in the ear canal,'' J. Acoust. Soc. Am. **86**, S44.
Puria, S., and Allen, J. B. (**1991**). ''A parametric study of cochlear input impedance,'' J. Acoust. Soc. Am. **89**, 287–309.
Puria, S., and Allen, J. B. (**1992**). ''SYSid—audio-band measurement and analysis system,'' J. Acoust. Soc. Am. **92**, 2469.
Puria, S., and Allen, J. B. (**1994**). Unpublished observations.
Puria, S., and Allen, J. B. (**1996**). ''Cat middle-ear measurements and model: Evidence of acoustic delay in the tympanic membrane,'' Assn. for Research in Oto-Laryngology Abstracts.
Puria, S., Peake, W., and Rosowski, J. (**1997**). ''Sound-pressure measurements in the cochlear vestibule of human-cadaver ears,'' J. Acoust. Soc. Am. **101**, 1–17.
Puria, S., Rosowski, J. J., and Peake, W. (**1993**). ''Middle-ear pressure gain in humans: preliminary results,'' in *Biophysics of Hair Cell Sensory Systems*, edited by H. Duifhuis, J. Horst, P. van Dijk, and S. van Netten (World Scientific, Singapore), pp. 345–351.
Rabbitt, R. D., and Holmes, M. H. (**1986**). ''A fibrous dynamic continuum model of the tympanic membrane,'' J. Acoust. Soc. Am. **80**, 1716–1728.
Rabbitt, R. D., and Holmes, M. H. (**1988**). ''Three-dimensional acoustic waves in the ear canal and their interaction with the tympanic membrane,'' J. Acoust. Soc. Am. **83(3)**, 1064–1080.
Shaw, E. A. G. (**1977**). ''Eardrum representation in middle-ear acoustical networks,'' J. Acoust. Soc. Am. **62**, E5.
Shaw, E. A. G., and Stinson, M. R. (**1981**). ''Network concepts and energy flow in the human middle ear,'' J. Acoust. Soc. Am. **69**, S44.
Shaw, E. A. G., and Stinson, M. R. (**1983**). *The Human External and Middle Ear: Models and Concepts* (Delft U.P., Delft, The Netherlands), pp. 3–10.
Shera, C. A., and Zweig, G. (**1991**). ''Phenomenological characterization of eardrum transduction,'' J. Acoust. Soc. Am. **90**, 253–262.
Shera, C. A., and Zweig, G. (**1993**). ''Noninvasive measurement of the cochlear traveling-wave ratio,'' J. Acoust. Soc. Am. **93**, 3333–3352.
Siebert, W. T. (**1970**). ''Simple model of the impedance matching properties of the external ear,'' MIT Research Laboratory of Electronics, Quarterly Prog. Rep. No. 96, 236–242.
Stinson, M. R., and Khanna, S. M. (**1994**). ''Spatial distribution of sound pressure and energy flow in the ear canals of cats,'' J. Acoust. Soc. Am. **96**, 170–180.
Tonndorf, J., and Pastaci, H. (**1986**). ''Middle ear sound transmission: A field of early interest to Merle Lawrence,'' Am. J. Otolaryngol. **7**, 120–129.
Voss, S. E., and Allen, J. B. (**1994**). ''Measurement of acoustic impedance and reflectance in the human ear canal,'' J. Acoust. Soc. Am. **95**, 372–384.
Wada, H., Metoki, T., and Kobayashi, T. (**1992**). ''Analysis of dynamic behavior of human middle ear using a finite-element method,'' J. Acoust. Soc. Am. **92**, 3157–3168.
Wever, E. G., and Lawrence, M. (**1950**). ''The acoustic pathways to the cochlea,'' J. Acoust. Soc. Am. **22**, 460–467.
Wever, E. G., and Lawrence, M. (**1954**). *Physiological Acoustics* (Princeton U.P., Princeton, NJ).
Zwislocki, J. (**1962**). ''Analysis of the middle-ear function. Part I: Input impedance,'' J. Acoust. Soc. Am. **34**, 1514–1523.
Zwislocki, J. (**1963**). ''Analysis of the middle-ear function. Part II: Guinea-pig ear,'' J. Acoust. Soc. Am. **35**, 1034–1040.